

12

DTIC FILE COPY

CHEMICAL  
RESEARCH,  
DEVELOPMENT &  
ENGINEERING  
CENTER

CRDEC-CR-87057

INVESTIGATION OF A COMPLEX TECHNIQUE  
OF SMOKE PARTICLE DEPOSITION ON  
SCAVENGERS

AD-A181 049

DTIC  
ELECTE  
JUN 04 1987  
S D  
D

by Josef Podzimek  
UNIVERSITY OF MISSOURI-ROLLA  
Rolla, MO 65401

March 1987

DISTRIBUTION STATEMENT A  
Approved for public release  
Distribution Unlimited



U.S. ARMY  
ARMAMENT  
MUNITIONS  
CHEMICAL COMMAND

Aberdeen Proving Ground, Maryland 21010-5423

87 6 2 9 1

Disclaimer

The findings in this report are not to be construed as an official Department of the Army position unless so designated by other authorizing documents.

Distribution Statement

Approved for public release; distribution is unlimited.

UNCLASSIFIED

SECURITY CLASSIFICATION OF THIS PAGE

AD-A181079  
REPORT DOCUMENTATION PAGE

1a. REPORT SECURITY CLASSIFICATION UNCLASSIFIED		1b. RESTRICTIVE MARKINGS	
2a. SECURITY CLASSIFICATION AUTHORITY		3. DISTRIBUTION/AVAILABILITY OF REPORT Approved for public release; distribution is unlimited.	
2b. DECLASSIFICATION/DOWNGRADING SCHEDULE		5. MONITORING ORGANIZATION REPORT NUMBER(S)	
4. PERFORMING ORGANIZATION REPORT NUMBER(S) CRDEC-CR-87057		7a. NAME OF MONITORING ORGANIZATION U.S. Army Research Office	
6a. NAME OF PERFORMING ORGANIZATION University of Missouri-Rolla	6b. OFFICE SYMBOL (if applicable)	7b. ADDRESS (City, State, and ZIP Code) P.O. Box 12211 Research Triangle Park, NC 27709	
6c. ADDRESS (City, State, and ZIP Code) Rolla, MO 65401	9. PROCUREMENT INSTRUMENT IDENTIFICATION NUMBER DAAK-11-83-K-0007		10. SOURCE OF FUNDING NUMBERS
8a. NAME OF FUNDING/SPONSORING ORGANIZATION CRDEC	8b. OFFICE SYMBOL (if applicable) SMCCR-RSP-B	PROGRAM ELEMENT NO.	PROJECT NO.
8c. ADDRESS (City, State, and ZIP Code) Aberdeen Proving Ground, MD 21010-5423		TASK NO.	WORK UNIT ACCESSION NO.
11. TITLE (Include Security Classification) Investigation of a Complex Technique of Smoke Particle Deposition on Scavengers			
12. PERSONAL AUTHOR(S) Podzimek, Josef			
13a. TYPE OF REPORT Contractor	13b. TIME COVERED FROM 83 Jun to 86 Aug	14. DATE OF REPORT (Year, Month, Day) 1987 March	15. PAGE COUNT 87
16. SUPPLEMENTARY NOTATION COR: Dr. G. Rubel, SMCCR-RSP-B, (301) 671-2326			
17. COSATI CODES		18. SUBJECT TERMS (Continue on reverse if necessary and identify by block number)	
FIELD	GROUP	Scavenging of military, smoke particles, Evolution, <del>of</del> falling, scavenger, zones, Aerodynamic, interaction, <del>of</del> falling scavengers	
24	01		
19. ABSTRACT (Continue on reverse if necessary and identify by block number) Numerical models were applied for assessing the smoke particle scavengers of simple geometry. The results were compared with experiments in laboratory wind tunnels and in a smoke chamber, where light extinction measurements were performed in a TiCl <sub>4</sub> cloud. Most effective scavengers were mesh type collectors and filter type material consisting of electrete fibers. Their maximum collection efficiency surpassed 10% for collectors bearing no additional electrical charges. The effect of this scavenging technique can be increased by appropriate combination of different types of fibers with respect to the specific (anticipated) aerosol size distribution.  For some of the selected types of scavengers the dispersion cone has been deduced experimentally and the behavior and aerodynamic interactions of falling scavengers described in calm air.			
20. DISTRIBUTION/AVAILABILITY OF ABSTRACT <input checked="" type="checkbox"/> UNCLASSIFIED/UNLIMITED <input type="checkbox"/> SAME AS RPT <input type="checkbox"/> DTIC USERS		21. ABSTRACT SECURITY CLASSIFICATION UNCLASSIFIED	
22a. NAME OF RESPONSIBLE INDIVIDUAL Timothy E. Hampton		22b. TELEPHONE (Include Area Code) (301) 671-2914	22c. OFFICE SYMBOL SMCCR-SPS-1

DD FORM 1473, 84 MAR

83 APR edition may be used until exhausted  
All other editions are obsolete

SECURITY CLASSIFICATION OF THIS PAGE

UNCLASSIFIED

## 19. Abstract (Continued)

Evolution of falling scavenger zone--essential for developing methodology of field experiments--has been described by numerical models for calm and light side wind condition. The main parameters important for generating an induced downdraft in the scavenger zone--contributing most to the clearing of the smoke cloud (e.g., the scavenger mixing ratio, zone initial dimensions) have been identified.



Blank

## CONTENTS

1. Introduction.....	7
2. Scavenger Collection Efficiency-Theoretical Study....	8
3. Experimental Investigation of the Clearing of a Smoke Cloud by "SPADES" Technique.....	23
4. Investigation of the Falling Scavenger Zone.....	32
5. Discussion of the Main Results.....	43
6. Conclusion.....	48
References.....	49
Appendixes	
A - Calculation of Particle Trajectories for Potential Flow.....	53
B - Viscous Flow Past an Infinite Cylinder.....	63
C - Two Hydrodynamically Interacting Cylinders.....	67
D - Brown's Model for Many-Fiber Viscous Flow.....	69
E - Physical Model for the Falling Scavenger Flow..	73

Blank

## INVESTIGATION OF A COMPLEX TECHNIQUE OF SMOKE PARTICLE DEPOSITION ON SCAVENGERS

### 1. INTRODUCTION

The research program "Investigation of a Complex Technique for Smoke Particle Deposition on Scavengers (SPADES)", DAAK-11-83-K-0007 concentrated on several promising results of the previous investigations under DAAK-11-81-C-0075 and DAAG-29-79-C-0073. It stressed the deposition of smoke particulates on nonspherical bodies which had shapes of planar scavengers (disks, plates, and grids), falling steadily or performing an oscillatory motion. Special attention was paid to the aerosol collection efficiency of scavengers made of fine electrete fibers organized in a regular mesh or forming a thick plate of randomly oriented fibers (Dust Magnet, Poly Mag 80 and 90, product of Brudhow Industries, Collierville, TN). These experiments were aimed at confronting the results of the numerical modeling of smoke particle deposition on uncharged and charged collectors with the measurement in a laboratory wind tunnel.

Most of the laboratory experiments have been performed with smoke particles generated by the reaction of titanium chloride with water vapor. This reaction with the subsequent particle shattering in an electric furnace yielded a narrow size distribution of smoke particles with the modus lying within the size range of "Greenfield gap" ( $0.2 \mu\text{m} < d < 0.8 \mu\text{m}$ ). The technique of aerosol generation has been described in the Final Report DAAK-11-81-C-0075. Our main task under this grant was to increase the reproducibility and duration of smoke particle generation for the investigation of particle deposition on models in a wind tunnel, or for the light extinction measurements in a smoke chamber.

One of the main tasks in the program DAAK-11-83-K-0007 was the investigation of the behavior of a cloud of falling scavengers in which the collectors do not interact hydrodynamically, however, as a whole they induce a downdraft. That on one side might entrain the smoke particles and transport them downwards, however, on the other side the decreasing relative velocity of a smoke particle and collector leads to the lowering of the collection efficiency of the scavenger.

Finally, an assessment of the total mass (number of scavengers of a specific type for improving the visibility in a smoke cloud was made. This assessment accompanied by a suggested scavenger dispersion over a smoke zone gives an idea about the practical applicability of the SPADES research program results.

## 2. SCAVENGER COLLECTION EFFICIENCY-THEORETICAL STUDY

The premise of this program was that a planar collector has a higher scavenging efficiency than a sphere (drop) of the same cross sectional area (Martin and Podzimek, 1982) and the same volume of displaced fluid. Because of the given size of smoke particles ( $0.2 < d_p < 1.0 \mu\text{m}$ ), the original model used by the investigators at UCLA (Pitter, 1977; Martin et al., 1980a, b, c) had to be modified and extended into the large Reynolds numbers and checked the suitability and additivity of terms describing the particle deposition by Brownian diffusion, phoretic and electrostatic forces.

Assuming that the mass of smoke particle,  $m_p$ , is much smaller than the mass of the collector (e.g., disk, grid) one can deduce the aerosol particle trajectory from the equation for the particle velocity,  $v_p$ ,

$$\frac{d \vec{v}_p}{dt} = m_p \vec{g} - \frac{6\pi\mu_a r_p}{(1+\alpha Kn)} (\vec{v}_p - \vec{u}_a) + \vec{F}_{Th} + \vec{F}_{Dif} + \vec{F}_B \quad (1)$$

This equation does not include the term corresponding to the effect of Brownian diffusion, which is applicable to particle radii,  $r_p < 0.1 \mu\text{m}$ . In a separate numerical model it was included earlier together with the effect of electrostatic charge by Martin et al. (1980c). However, the terms for Brownian diffusion, thermo- and diffusiophoretic forces can be neglected in comparison to the effect of inertial and electric forces for the  $\text{TiCl}_4$  smoke particles of the size distribution curve analysed and published earlier (Podzimek, 1983). For the same reason the slip flow correction term  $\alpha Kn$  with  $\alpha = 1.26 + 0.44 \times \exp(-1.10 \text{Kn}^{-1})$  and  $Kn = \frac{\lambda}{r_p}$  can be neglected.

From the known particle trajectory around the disk (thin oblate spheroid with axes ratio of 0.05) the disk collision efficiency

$$E = \frac{\pi Y_c^2}{\pi (r_c + r_p)^2} \quad (2)$$

was deduced.  $Y_c$  is the largest offset of the particle from the disk's main axis the particle can have and still collide with the crystal. No attempt was made to speculate about the potential "annular effect" decreasing the number of deposited particles around the stagnation point on the obverse side of the disk (Pitter and Pruppacher, 1974).

A composite diagram for different  $Re$  (up to  $Re = 80$ ), uncharged particulates is presented in Fig. 1. It assumes the validity of Eq. (1) in which phoretic terms ( $F_{Th}$ ,  $F_{Dif}$ ) and Brownian diffusion are small in comparison to the inertial deposition for particle radii greater than  $0.1 \mu\text{m}$ . The formulas for creeping flow conditions and for the forces acting on an

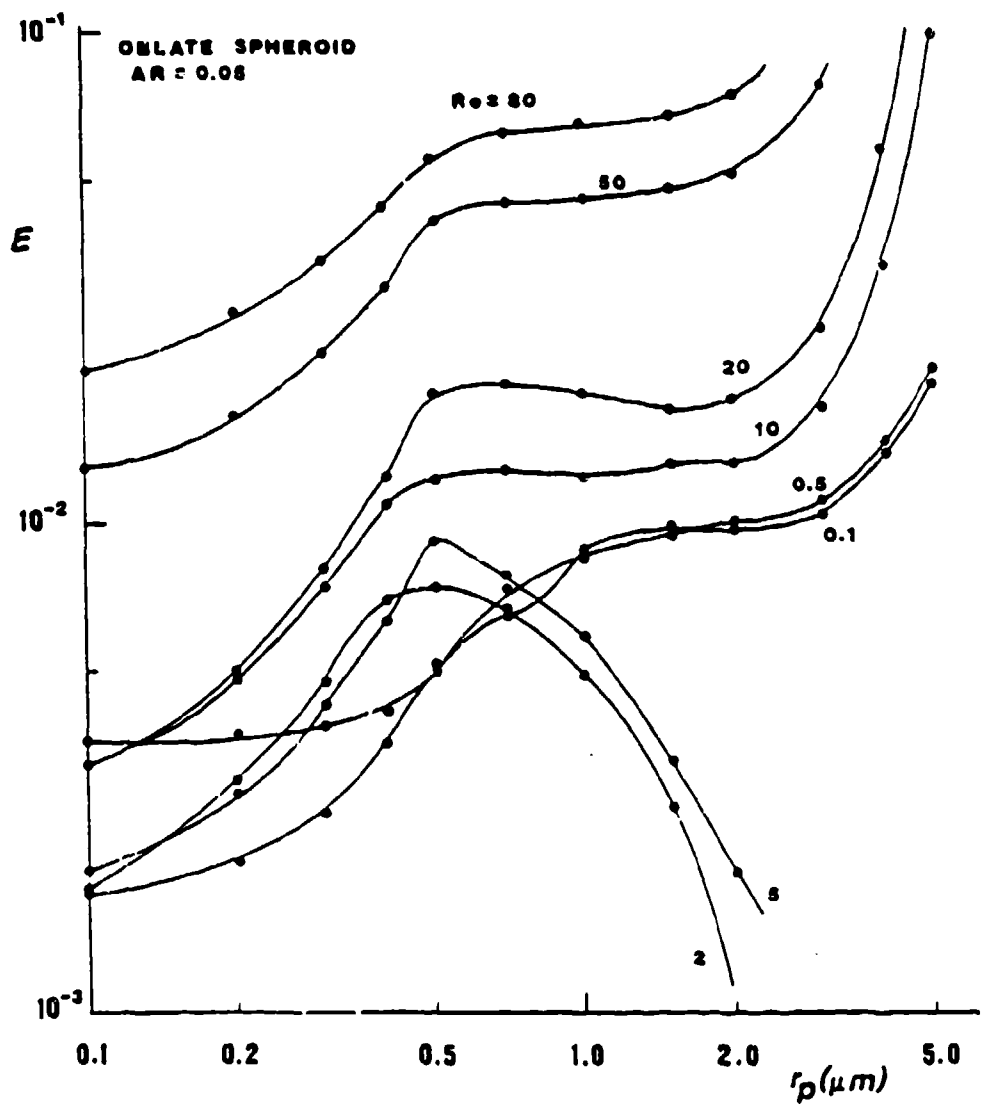


Fig. 1 Diagram of collision efficiencies of oblate spheroid (AR = 0.05) scavengers as a function of smoke particle radius,  $r_p$  [ $\mu m$ ] and Re.

aerosol particle were described elsewhere (Martin et al, 1980a, 1980b, 1980c; Martin and Podzimek, 1982; Podzimek, 1983). The most significant result one can deduce from Fig. 1 based on the theoretical calculations for a disk is that the collection efficiency for smoke aerosol particles (with radii between 0.1  $\mu\text{m}$  and 2.0  $\mu\text{m}$ ) will not surpass 8%. The inertial deposition will be the main mechanism for smoke particle scavenging with a considerable influence of thermophoretic forces (if they exist) in the particle size range  $0.3 < r_p < 0.8 \mu\text{m}$ . The only explanation of the peculiar behavior of particles at  $Re = 0.1$ ; 0.5 and 1.0 (which shows  $E < 10^{-3}$  for all particle sizes considered and therefore is not drawn in Fig. 1) is the basic change of the flow pattern around the oblate spheroid at low  $Re$  and the evolution of vortices on the reverse side at  $Re > 5.0$ . At  $Re < 0.5$  particle laden air is longer time in contact with the collectors surface.

Much attention has been paid to the analysis of different kind of electric charging of the collector and smoke particle as well and to its effect on collection efficiency of a planar collector (Podzimek and Martin, 1984). In spite of the fact that both field and diffusion charging might affect the particle deposition a simplified model was applied to the force acting on aerosol particle in the proximity of the scavenger

$$\vec{F}_{1,2} = m_1 \vec{g}^* - \frac{6\pi \eta_a r_1}{(1+2 Kn)} (\vec{V}_1 - \vec{V}_2) + K_1 \vec{\nabla} T + K_2 \vec{\nabla} \rho_v + O_1 \vec{E}_2 \quad (3)$$

and on the collector due to the image charge induced by the smoke particle

$$\vec{F}_{2,1} = m_2 \vec{g}^* - \frac{6\pi \eta_a r_2}{(1+2\alpha Kn)} (\vec{V}_2 - \vec{V}_1) + K_1 \vec{\nabla} T + K_2 \vec{\nabla} \rho_v + O_2 \vec{E}_1 \quad (4)$$

The terms in each equation represent the buoyancy corrected gravitational force, corrected drag in accordance with Stokes resistance law (assumption is made that the effect of planar and spherical collector are similar). Further it was assumed that the scavenger position and orientation of the collector's axes remains undisturbed by either hydrodynamic interaction of particles or by electrical forces (Martin et al, 1981). The Coulomb forces are the dominant ones and are radiating from the mass center of each body (image forces are not considered). The justification of creeping flow equations and the numerical technique for a thin oblate spheroid has been discussed by Martin et al. (1980b). Under this program additional flow fields for  $Re = 80$  were developed. There were considerable difficulties with a similar model for  $Re = 100$  due to the flow instability. In case that there is no evaporation or vapor condensation on smoke particles, the diffusio-phoretic and thermophoretic terms were set to zero. The collection efficiency curve for  $Re = 80$  is compared to the old curves (Martin and Podzimek, 1982) for low  $Re$  and plotted in Fig. 2. In conclusion, the electric charge effect can dramatically change the particle deposition on a charged

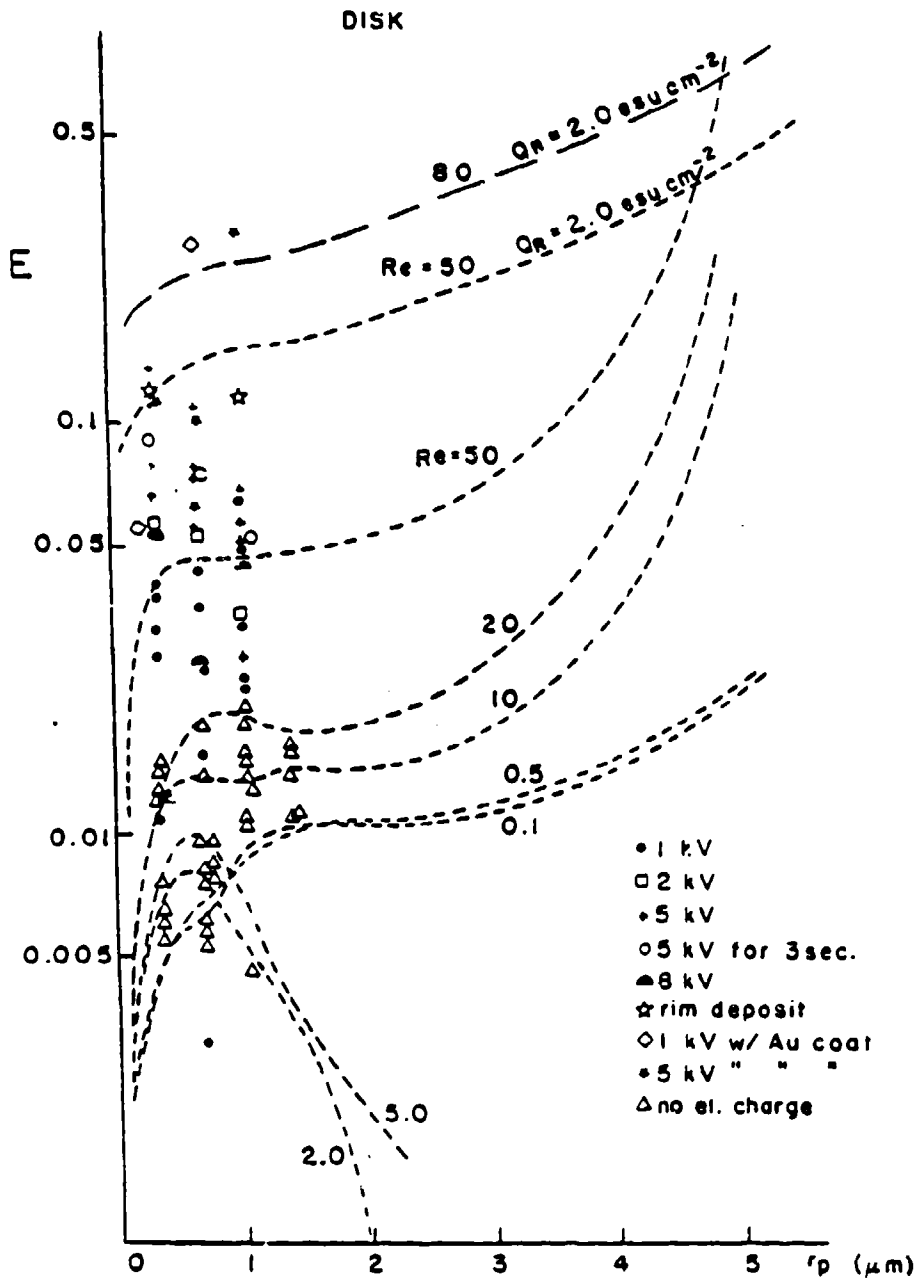


Fig. 2 Collision efficiency of charged and uncharged oblate spheroid (disk) as a function of  $Re$ , particle radius,  $r_p$ , and electric charge.

collector. The surface charge assumed in our calculation is high ( $Q_s = 2.0 \text{ esu cm}^{-2}$ ) indeed ( $2.0 \text{ esu cm}^{-2}$ ) and it can be hardly maintained in a dense aerosol cloud. At the beginning of the particle deposition it might enhance the particle deposition of one order of magnitude. The other interesting feature of the assumed positive interaction of smoke particles with a charged collector is the inefficiency of such a process for particulates with radii larger than  $5.0 \mu\text{m}$  if compared to the collision of not electrically charged particles. This is also apparent in Fig. 3 where is plotted the calculated collision efficiency of a thin oblate spheroid as a function of Stokes number,  $K$ .

Considerable effort has been made to investigate the collision efficiency of cylinders (fibers). The collision efficiencies calculated from models presented by different authors are plotted in Fig. 4. There is still a considerable uncertainty of different models in the domain of low  $Re$ , however, it can be shown that our data (curve 4 in Fig. 1) for potential flow are not much different from the calculation by Davies and Peetz or from the stepwise calculation by Harrop (using Happel flow field) - curve 1 in Fig. 4. The calculation of the flow field and particle trajectories are presented in Appendix A. There is still a gap in our knowledge of the ultrafine particle deposition in a viscous flow around a very fine fiber, what would mean to extend our curves in Fig. 4 into the domain of Stokes numbers  $K \leq 0.01$ . For instance, the Kuwabara model--used by several authors and supported roughly by experiments (Kirsch and Fuchs, 1967) for the determination of particle trajectories around a fiber--is too sensitive to the starting conditions. The same holds for the model used by Schlamp (1977) for calculation of cloud droplet deposition on columnar type crystals, which the author approximated by infinite cylinder (Appendix B).

The main results of the investigation (Liu, 1985) for ideal flow without electrostatic force and aerosol particles negligibly small compared with the cylinder can be summarized as follows: There is a reasonably good agreement between our data and the collision efficiency calculated by Albrecht (1931), Sell (1931) and Glauert (1940), Langmuir and Blodgett (1946) and Davies and Peetz (1955) for the cylinder in the transition flow region (Fig. 5). The slight disagreement of the curves can be explained by the higher sensitivity of the numerical calculation with respect to the starting point ahead of the cylinder. Glauert and Sell and Albrecht started at three cylinder diameters where they assumed aerosol particles having the same velocity like an airflow at infinity. Langmuir and Blodgett started at four and Davies and Peetz at five diameters. In our case we selected six diameters and hoped to obtain sufficiently accurate particle trajectory along the obverse side of a cylinder. Another reason for the disagreement of curves in Fig. 5 might be the different particle density assumed by the investigators. In Fig. 6 are plotted the particle trajectories about a cylinder positively charged, uncharged and negatively charged. This causes a  $5.0 \mu\text{m}$  (radius) particle to be repulsed or attracted close to the

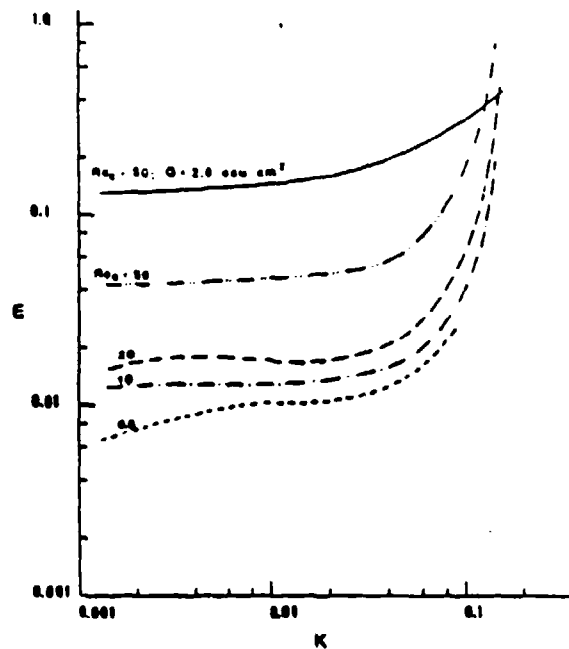


Fig. 3 Calculated collision efficiency of a thin oblate spheroid as a function of  $Re$  and Stokes number,  $K$ .

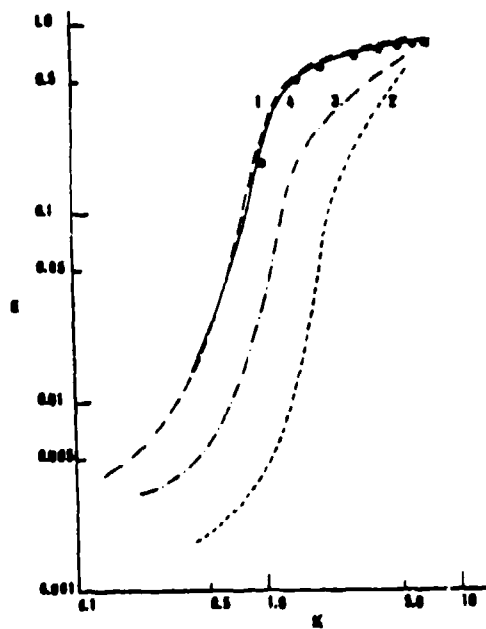


Fig. 4 Calculated collision efficiency,  $E$ , of an infinite cylinder as a function of Stokes number of particles,  $K$ , by different authors.

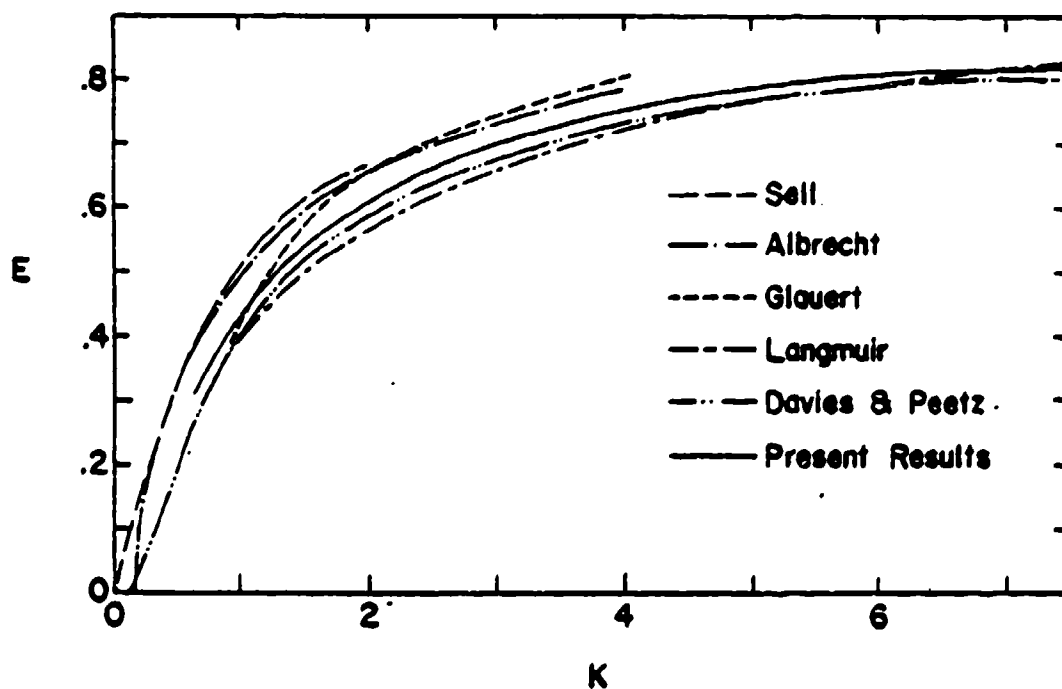


Fig. 5 Comparison of theoretical collision efficiencies for a circular cylinder and aerosol particles as a function of Stokes number.

surface of a metallic cylinder in addition to the action of inertial forces. The particle density,  $\rho_p = 1.0 \text{ g cm}^{-3}$  in this case, plays an important role in modifying the trajectory and the number of deposited particles, as it is demonstrated in Fig. 7, where for comparison, the particle trajectories are plotted for  $\rho_p = 2.0 \text{ g cm}^{-3}$ . The effect of positively and negatively charged collector on the aerosol particle (of the same size mass and charge) collision is different (in Fig. 8 are plotted the collision efficiencies for the example case described in Fig. 6). The comparison of Figs. 6 and 7 leads also to the conclusion that for enough strong attractive Coulomb force the collision efficiency will be getting larger for smaller particle density ( $\rho_p = 1 \text{ g cm}^{-3}$ ). For repulsive Coulomb force the situation reverses if the electric charge force overrides that of the inertial force.

For the sake of estimating the potential effect of the hydrodynamic interaction of two cylinders in the transition flow region, we studied the particle deposition on two cylinders close together. The main results of these theoretical studies--which are described in more detail in Appendix C--can be summarized as follows: Collision efficiencies for an example case ( $U_c = 0.1 \text{ cm}$ ,  $U = 100 \text{ cm s}^{-1}$ ,  $\rho_p = 1.0 \text{ g cm}^{-3}$ ) of particle deposition in potential flow are increasing with diminishing distance between cylinder (fiber) centers,  $S$ , until approximately  $S/D_c = 2.0$ , and then decrease with smaller value of  $S/D_c$  (Fig. 9).<sup>C</sup> At a value  $S/D_c \approx 1.2$  the two parallel fibers act approximately like a single body (Shyu, 1986).

An attempt was made to substitute a rather unrealistic application of a potential flow to the not very close packed parallel fibers by a model simulating an airflow through a many fiber array forming a rectangular net (channel model) or a staggered model (Brown, 1984). These models are substituting the stream functions suggested by Kuwabara (1959), Happel (1959) or Spielman and Goren (1969) of the type

$$\psi = \frac{\bar{U}R}{2\xi} \left( \frac{R}{r} - \frac{r}{R} + 2 \frac{r}{R} \ln \frac{r}{R} \right) \sin\theta, \quad (5)$$

where  $\xi$  is a specific hydrodynamic factor, by many - fiber term

$$\psi = \bar{U}_x y + \bar{U}_x \ell \sum_{n=1}^{\infty} \sum_{k=0}^{\infty} a_{nk} \sin \frac{n\pi y}{\ell} \cos \frac{k\pi x}{e} \quad (6)$$

The many-fiber stream function reflects (in the form of double Fourier series in  $x$  and  $y$ ) the spacial periodicity and might be suitable for the investigation of smoke particle deposition on filter type electrete fiber scavengers. The meaning of the geometrical parameters  $\ell$  and  $e$  is apparent from the description in Appendix D. In conclusion, it seems suitable to our task of investigating the deposition of smoke particulates on fiber type

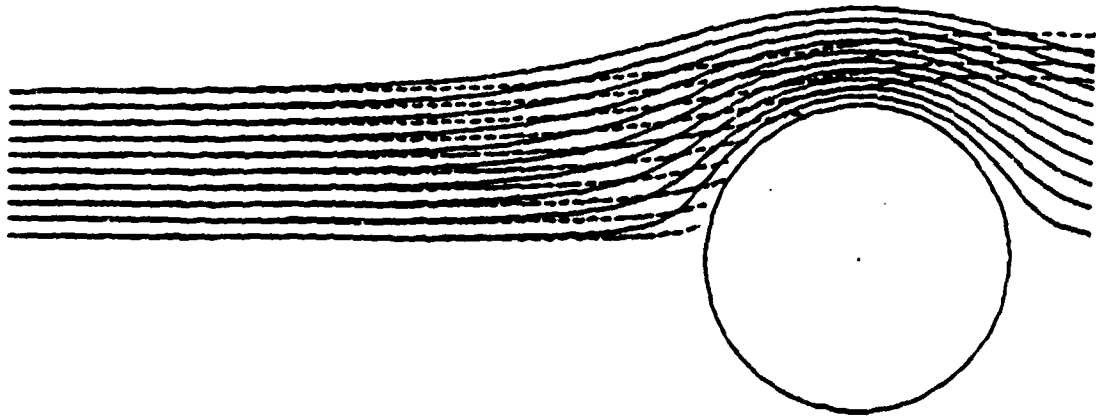


Fig. 6a Particle trajectory without electrostatic force,  $\rho_p = 1.0 \text{ g/cm}^3$ .  $D_c = 0.05 \text{ cm}$ ,  $D_p = 10 \text{ }\mu\text{m}$ ,  $N_{Re} = 55$ ,  $AR = 1/6$ .

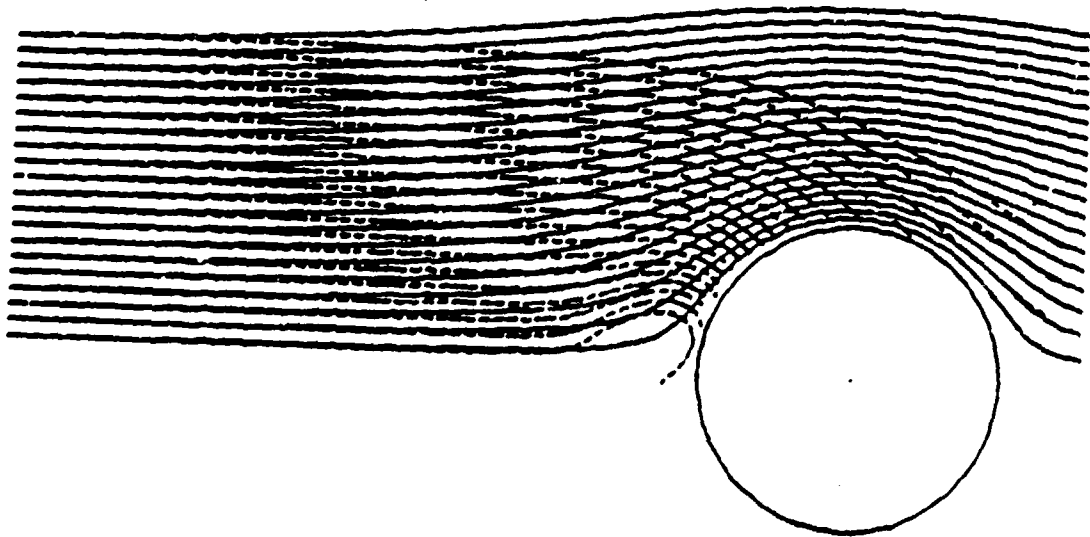


Fig. 6b Particle trajectory with attractive force,  $\rho_p = 1.0 \text{ g/cm}^3$ .  $D_c = 0.05 \text{ cm}$ ,  $D_p = 10 \text{ }\mu\text{m}$ ,  $N_{Re} = 55$ ,  $AR = 1/6$ ,  $Q_A = 7.5 \times 10^{-2} \text{ e.s.u.}$  ( $Q_A' = 20$ ),  $Q_B = -5.0 \times 10^{-6} \text{ e.s.u.}$  ( $Q_B' = -20$ ).

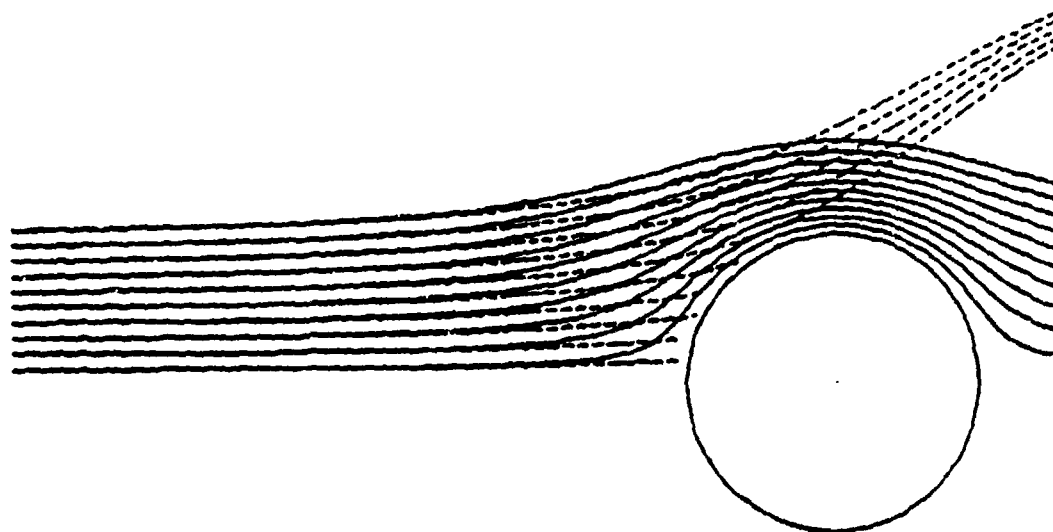


Fig. 6c Particle trajectory with repulsive force,  $\rho_p = 1.0 \text{ g/cm}^3$   
 $D_c = 0.05 \text{ cm}$ ,  $D_p = 10 \text{ }\mu\text{m}$ ,  $N_{Re} = 55$ ,  $AR = 176$ ,  $Q_A = 7.5 \times 10^{-2} \text{ e.s.u.}$  ( $Q_A' = 20$ ),  $Q_B = 5.0 \times 10^{-6} \text{ e.s.u.}$  ( $Q_B' = 20$ ).

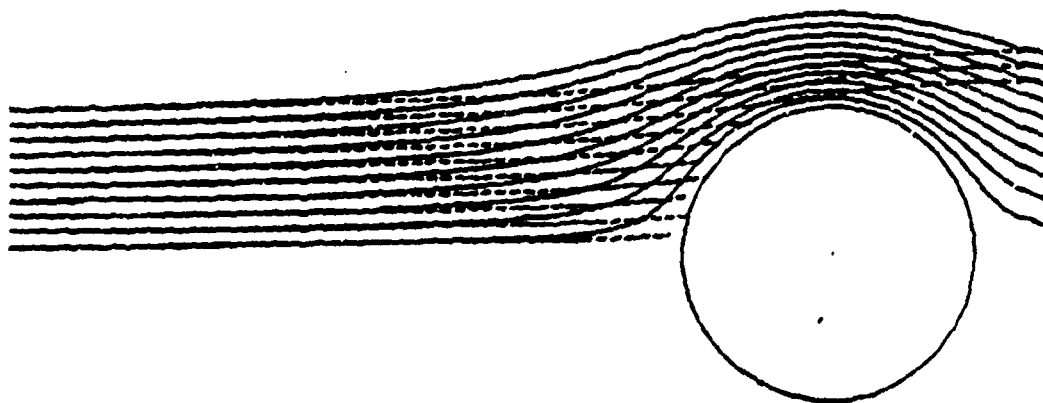


Fig. 7a Particle trajectory without electrostatic force,  $\rho_p = 2.0 \text{ g/cm}^3$ .  $D_c = 0.5 \text{ cm}$ ,  $D_p = 10 \text{ }\mu\text{m}$ ,  $N_{Re} = 55$ ,  $AR = 1/6$ .

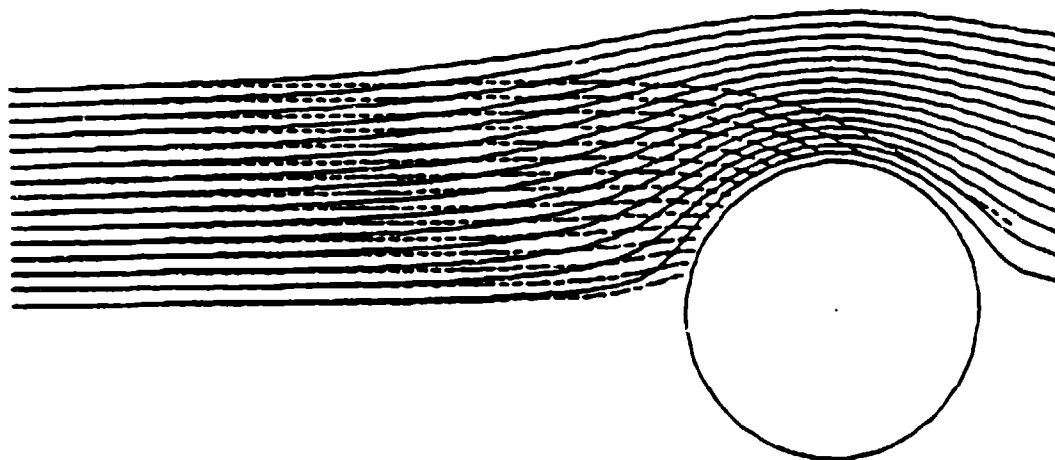


Fig. 7b Particle trajectory with attractive force,  $\rho_p = 2.0 \text{ g/cm}^3$ .  
 $D_c = 0.05 \text{ cm}$ ,  $D_p = 10 \text{ }\mu\text{m}$ ,  $N_{Re} = 55$ ,  $AR = 1/6$ ,  $Q_A = 7.5 \times 10^{-2} \text{ e.s.u.}$  ( $Q_A' = 20$ ),  $Q_B = -5.0 \times 10^{-6} \text{ e.s.u.}$  ( $Q_B' = -20$ ).

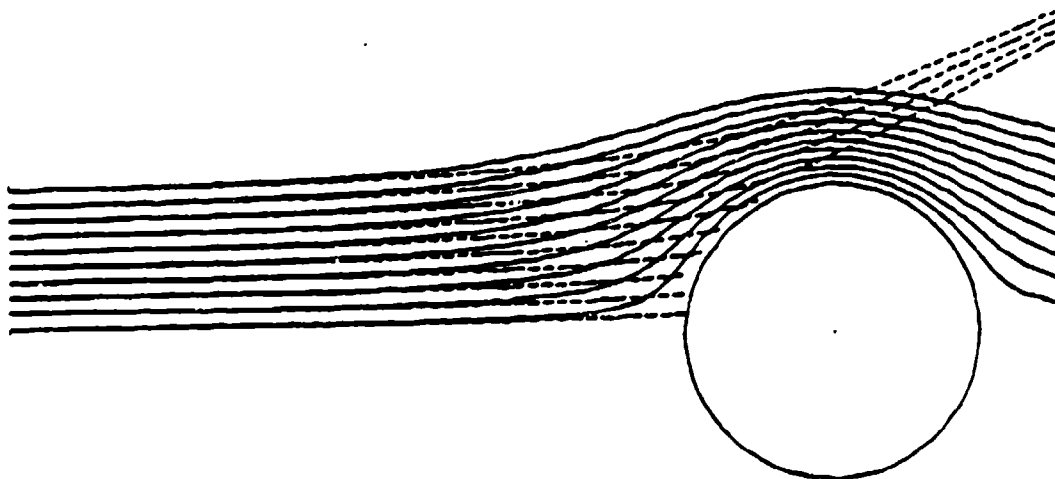


Fig. 7c Particle trajectory with repulsive force,  $\rho_p = 2.0 \text{ g/cm}^3$ .  
 $D_c = 0.05 \text{ cm}$ ,  $D_p = 10 \text{ }\mu\text{m}$ ,  $N_{Re} = 55$ ,  $AR = 1/6$ ,  $Q_A = 7.5 \times 10^{-2} \text{ e.s.u.}$  ( $Q_A' = 20$ ),  $Q_B = 5.0 \times 10^{-6} \text{ e.s.u.}$  ( $Q_B' = 20$ ).

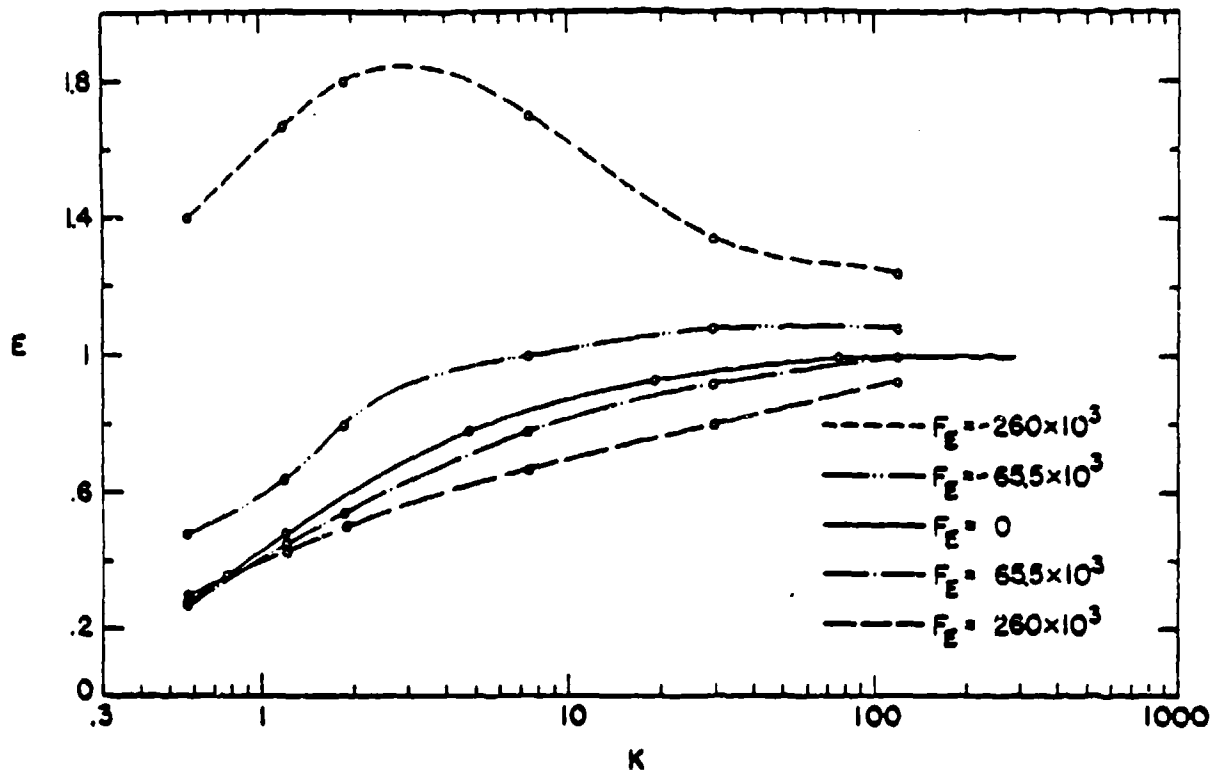


Fig. 8 Numerical collision efficiency  $E$  as a function of particle Stokes numbers  $K$  and  $D_C = 0.05$  cm,  $N_{Re} = 55$ ,  $\rho_p = 1$  g/cm<sup>3</sup> and  $AR = 1/6$ .

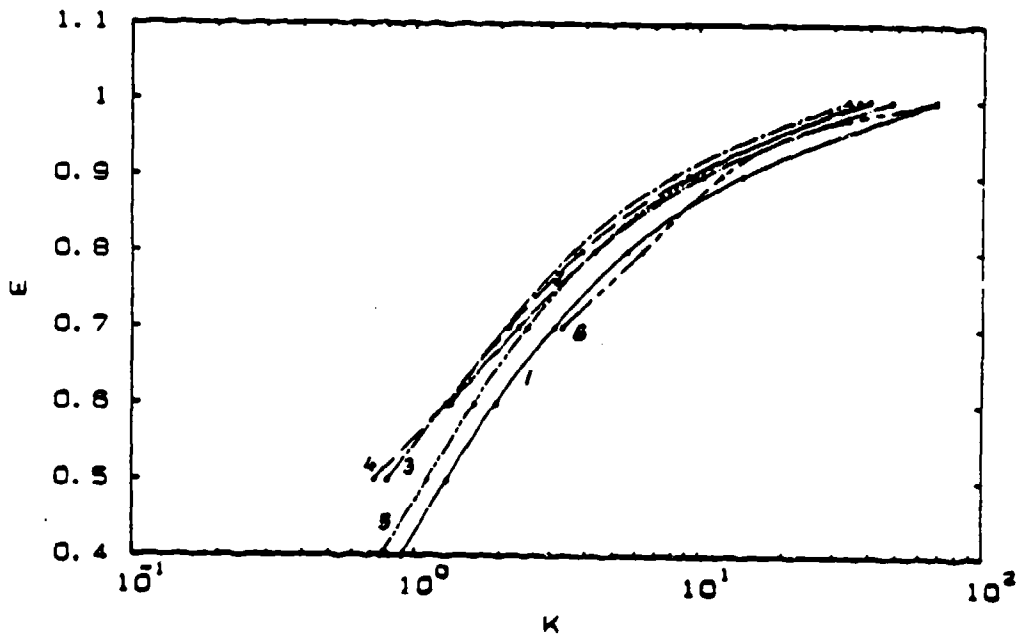


Fig. 9 Collision efficiency of interacting cylinders in potential flow:  $D_c = 0.1$  cm,  $U = 100$  cm  $s^{-1}$ ,  $\rho_p = 1.0$  g  $cm^{-3}$ . Distances of cylinder centers are in cm: 1(1), 0.5(2), 0.2(3), 0.17(4), 0.15(5), 0.12(6) curve.

scavengers, to develop further Brown's model because the model is relatively simple and it gives a reasonably good description of the flowfield. The last statement is based on Brown's analysis and on our preliminary experience which showed also a limited applicability of the model for thick filter material (pressure drop and changing Re across the filter). The inaccuracy of the model very close to the fiber surface does not affect much the deposition of particles the size of which excludes a strong influence of diffusional deposition. A more complicated expression for stream function will be required for a staggered model of a filter (Brown, 1984),

$$\psi = \bar{U}_x y + \bar{U}_x \ell \sum_{\text{odd } n=1}^{\infty} \sum_{k=0}^{\infty} a_{nk} \sin \frac{n\pi y}{\ell} \cos \frac{(2k+1)\pi x}{2e} +$$

$$+ \bar{U}_x \ell \sum_{\text{even } n=2}^{\infty} \sum_{k=0}^{\infty} a_{nk} \sin \frac{n\pi y}{\ell} \cos \frac{k\pi x}{e}, \quad (7)$$

which with corresponding boundary values will enable to calculate the flowfield in the array of fibers described in Appendix D.

The rate of smoke particles deposited on each row plan perpendicular to airflow direction can be calculated according to the formula

$$\frac{dn_j(r_{pi}, t)}{dt} \Big|_j = -2R L N_R \Delta \bar{V}_{Rj} n_j(r_{pi}, t) E(R_1 r_1 \rho_p) \quad (8)$$

which, after integration, yields

$$n_j(r_{pi}, t) = n_j(r_{pi}, 0) \exp(-\Lambda_{ij} t)$$

where

$$\Lambda_{ij} = \sum P_k \int_0^{r_{ps}} 2 R L E_j(R_i r_{pi}, U, W) (V_{Rj} - v_{pi}) N_{Rj} dr_{pi}$$

R, L, are radius and length of the fiber. P<sub>k</sub> is the probability of a specific position of the fiber (if they<sup>k</sup> are not parallel), E<sub>j</sub>(R<sub>i</sub>, r<sub>pi</sub>, U, W); ΔV<sub>Rj</sub> = (V<sub>Rj</sub> - v<sub>pi</sub>) is relative velocity particle-fiber, N<sub>Rj</sub> is the number of fibers of radius R in a plane j. The second row will start to scavenge of the depleted concentration

$$n_{j+1}(r_{pi}, t) = [1 - n_j(r_{pi}, t)] \exp(-\Lambda_{ij+1}t)$$

and for a constant  $\Lambda_{ij} \equiv \Lambda_{ij+1} \equiv \Lambda_{ij+2} \equiv \Lambda$  and the same time interval  $t_1$ , the number of smoke particulates remaining in the airflow after passing e.g., four planes of fibers will be

$$n_{rem}(r_{pi}, 4t) = n(r_{pi}, 0) [1 - \exp(-\Lambda, t) + \exp(-2\Lambda .t) - \exp(-3\Lambda .t) + \exp(-4\Lambda.t)] - 3 \exp(-\Lambda.t) + 2 \exp(-2\Lambda.t) - \exp(-3\Lambda.t) . \quad (9)$$

This model, which assumes that there is not a considerable pressure drop on individual fiber planes seems to be very appropriate to any type of filter or grid type scavenger where the assumption of parallel fibers is acceptable. The problem of grid type scavengers with node points or the effect of randomly oriented fibers requires further study.

### 3. EXPERIMENTAL INVESTIGATION OF THE CLEARING OF A SMOKE CLOUD BY "SPADES" TECHNIQUE

Smoke particle deposition on scavengers (SPADES) was investigated mainly in the laboratory wind tunnel and in the cylindrical smoke chamber (1.6 m high and 0.8 m in diameter). The aim of these experiments was the following: To complete the studies made under the U.S. Army Research Office Grants DAAG 29-79-C-0075 and DAAK 11-81-C-0075, and to concentrate mainly on grid type scavengers and planar scavengers made of electrete type fibers. These fibers were much more effective than solid planar scavengers (e.g., disk), the collection efficiency of which was about one or two percent for  $\text{TiCl}_4$  smoke particles with modus diameter around  $0.4 \mu\text{m}$ . An oscillatory motion did enhance only slightly the collection efficiency of thin disks (Podzimek, 1983).

Electrete type fibers showed high collection efficiency (7% for particle diameters smaller than  $0.5 \mu\text{m}$  at an airflow velocity of  $0.25 \text{ m s}^{-1}$ ). This indicates the important role played by the diffusion and electrostatic charge. The additional charging of electrete fibers will not enhance dramatically the deposition of smoke particles with diameters smaller than  $1.0 \mu\text{m}$  (Fig. 10). For the same electrete fiber diameter ( $0.004 \text{ cm}$ ) a higher flow velocity ( $1 \text{ m s}^{-1}$ ) stressed a little more the effect of the additional electrostatic charge, however, the total effect was smaller than in the previous case--in maximum 6.5% (5% for uncharged fiber) for particle diameters smaller than  $0.5 \mu\text{m}$  (Fig. 11). The other very important effect is the changing of size distribution curve of smoke particles which, after the first dropping of electrete scavengers, will remain in the air. Scavenger fibers analyzed under a scanning electron microscope reveal that size spectrum of particles found on the fiber is shifted towards larger sizes, and in consequence of that, in the air will remain smaller particles (Fig. 12). This result could be anticipated, however, what is the most important, that this shifting in smoke particle size distribution would require the use of different scavengers (e.g., the use of fast falling coarse fiber scavengers first and then dropping of finer electrete fibers of small settling velocity enhancing more deposition of fine particles by diffusion). The other possibility of using the most effective scavengers is to combine planar coarse fiber scavengers with fine fiber net stretched over the coarse fibers in order to remove the largest portion of the aerosol size spectrum (on this point a Patent Application will be submitted soon, through the U.S. Army authorities).

The very important part of experiments was the assessment of the reproducibility of the measured collection efficiency of mesh type scavengers in the laboratory wind tunnel and in the  $0.8 \text{ m}^3$  smoke chamber. The first task was closely related to the

Fig. 10 Comparison of collection efficiencies,  $E$ , for "Dust Magnet" fiber at different electrostatic charges and at the airflow of  $0.25 \text{ m s}^{-1}$ .

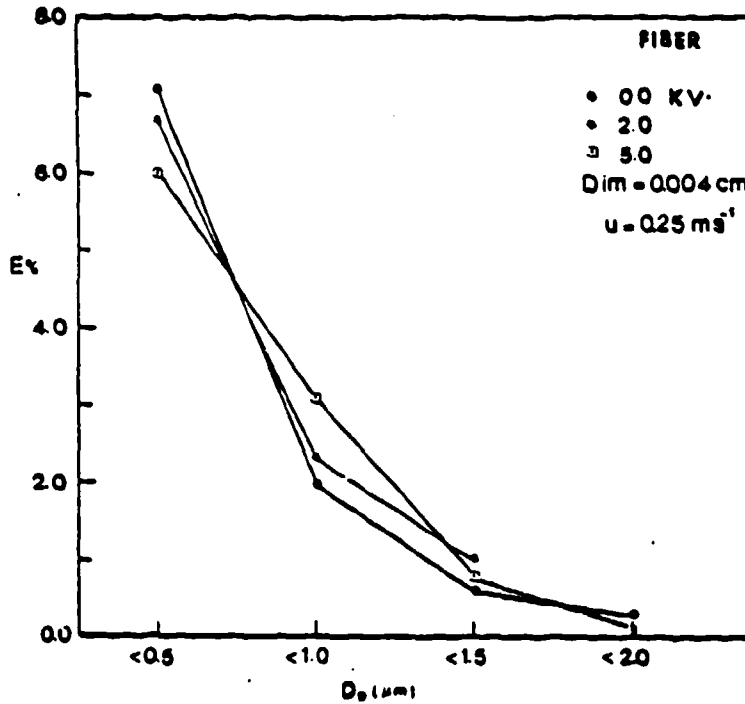
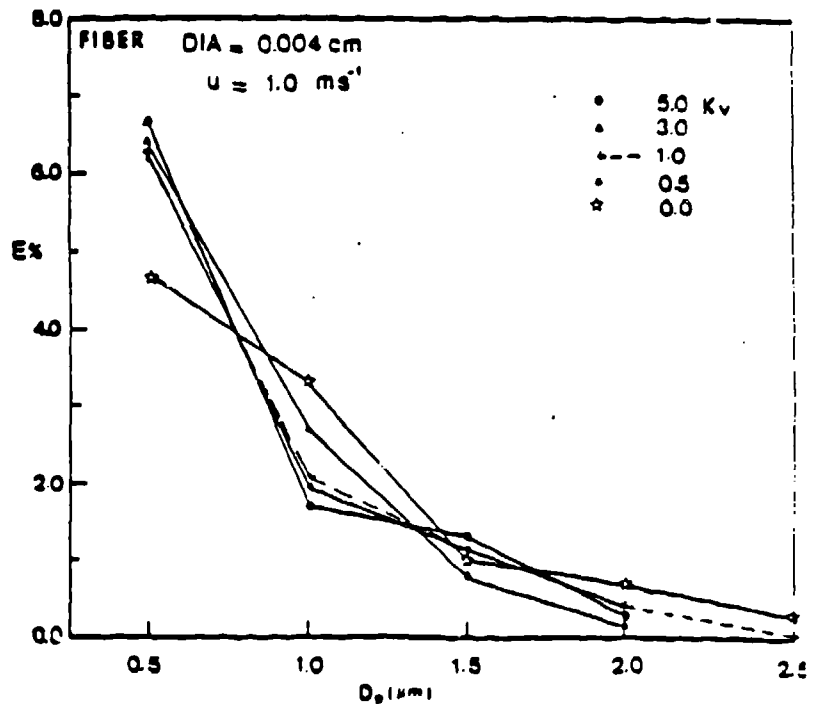


Fig. 11 Comparison of collection efficiencies,  $E$ , for "Dust Magnet" fiber at different electrostatic charges and at the airflow of  $1.0 \text{ m s}^{-1}$ .



standardization of the  $TiCl_4$  smoke particle generation--which is now controlled during each experiment in the wind tunnel within an error of approximately  $\pm 20\%$  of concentration in the main particle size groups. This task prompted new series of measurements which led to the special one-year research program supported by the University of Missouri the goal of which is the use of neutron activation analysis for determining the number and total mass of deposited Ti-containing particles on electrete fibers. The first pilot experiments done in 1986 partly within the DAAK-11-83-K-0007 program were very promising. In general it is expected that the neutron activation performed in the reactor of UMR will enable to detect small quantities of Ti containing particles down to  $0.10 \mu g$ , with a mean error of around  $\pm 10\%$ . This quantity combined with the use of laser cavity aerosol spectrometer for particle size distribution measurement represents a substantial improvement of the technique for the determination of the scavenger collection efficiency. The final report on the new measuring technique of smoke particle deposition on the fibers (UMR grant) will be sent to the U.S. Army Research Office during the year 1987.

More difficult was the assessment of the accuracy and reproducibility of measuring the visibility in a smoke chamber after a specific number of scavengers was dropped into a dense  $TiCl_4$  smoke cloud. Besides the smoke particle generation technique (described in the DAAK 11-81-C-0075 and DAAG 29-79-C-0073 reports) the following factors affect the measurement of visibility (instrumentation has been described also in the previous reports) in the smoke chamber: The type of scavenger, the art of scavenger dropping (frequency of individual droppings, dropping of scavenger groups in specific time intervals), width of the light beam for visibility measurement (probability of a scavenger crossing the light beam), size of the smoke chamber (air or smoke circulation induced by the falling scavengers) and the model used for analysis and interpretation of the measured visual range.

Most of the experiments have been done by the electrete denoted as "Dust Magnet" Poly-Mag 80 and 90, a product of Bruhow Industries, Collierville, TN. Several studies have been done with paper disks and squares described elsewhere (Podzimek, 1981). The coarse electrete fibers  $200-300 \mu m$  in diameter were arranged in a grid type array  $2.5 \text{ cm} \times 2.5 \text{ cm}$  (or  $1.25 \text{ cm} \times 1.25 \text{ cm}$ ) in size in which fibers of a mean diameter of  $250 \mu m$  are alternating with gaps of approximately  $500$  to  $750 \mu m$ . The mean scavenger mass was  $0.105 \text{ g}$  and the fall velocity of  $176 \text{ cm s}^{-1}$ . The filter type scavenger had dimensions  $2.5 \text{ cm} \times 2.5 \text{ cm}$ , x  $1.3 \text{ cm}$  (or  $1.25 \text{ cm} \times 1.25 \text{ cm} \times 0.7 \text{ cm}$ ). The dense packed fine fibers (approximately  $40 \mu m$  in diameter) were randomly oriented and the scavenger had a settling velocity similar to the coarse one. The main aim of these experiments was to estimate the total clearing effect in a dense smoke cloud after a specific number of scavengers was released and to relate these observations to the measurement in a wind tunnel. Another important goal of these

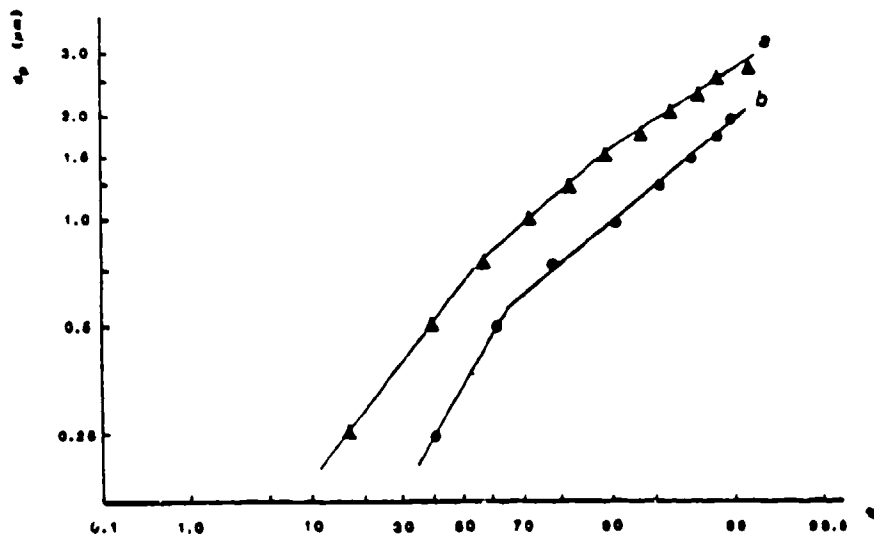


Fig. 12 Size spectrum of  $TiCl_4$  particles: a - deposited on the fiber, b - in the airflow.

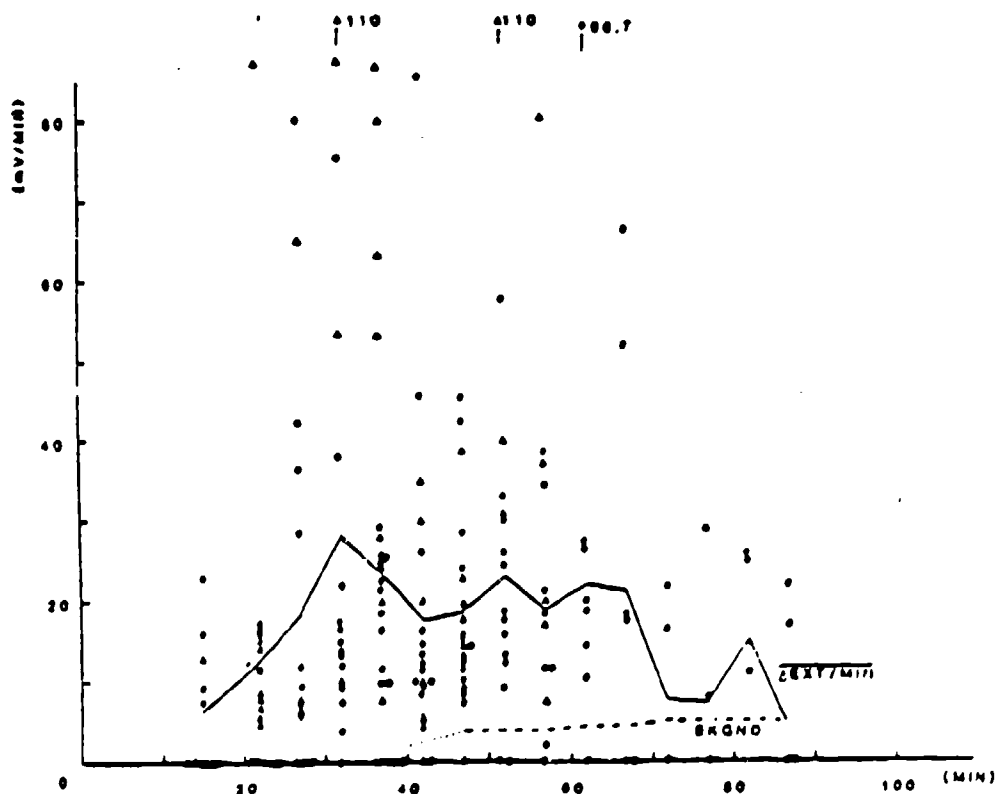


Fig. 13 Change in light extinction in a smoke cloud ( $\Delta ext/min \equiv mV/min$ ) was caused by dropping a specific number of scavengers in 5 minute intervals. Triangles correspond to fine fiber "Dust Magnet" scavengers, dots to the coarse fibers.

investigations was to find the optimal groups of scavengers with the highest scavenging efficiency and to find the most suitable time intervals between the dropping of scavengers. Typical size distribution curve (cumulative size spectrum curve) is presented in Fig. 12. There is clearly a broken line concave upwards--which supports strongly the observations made in a wind tunnel earlier.

All data from visual range (extinction) measurements are summarized in Fig. 13. It shows clearly that there is a significant improvement of visibility in a dense smoke (particle concentrations surpassed often  $500,000 \text{ cm}^{-3}$ ). The time change in light extinction is measured in relative units (mV/min). There is not much difference in light extinction caused by coarse fiber and fine (close packed) scavengers what supports our finding during the wind tunnel testing. In spite of a large spreading of data points there is a markable difference between the extinction background (measured before the scavengers were dropped), marked by a dashed line in Fig. 13, and the measured extinction after the scavengers passed the sensitive volume of the beam emitted from a light source. LED columnated source ( $\lambda = 6700 \text{ \AA}$ ) formed a light beam of 1.5 cm diameter and 80 cm length. The light intensity was monitored by Bell and Howell, Model 529, Photodiode Detector with a Transmission Meter. During a series of 46 measurements the most significant effect ( $\Delta V > 10 \text{ mV/min}$ ) was observed immediately after the first scavenger group was dropped and lasted approximately for 1 hour. The number of scavengers dropped usually during 5 minute intervals varied between 10 and 150 scavengers. There is a strong indication that the highest scavenger dropping rate (30 scavengers/min) did not cause the most significant change in light extinction. In general, dropping of scavengers in smaller groups with long intermissions was more effective. This indicates that the scavenger hydrodynamic interactions and air entrainment--which lowers considerably the collection efficiency of scavengers--might affect considerably the experiments in a smoke chamber of limited volume. For this reason it is not possible--at this time--to describe by a theoretical model the nature of smoke particle deposition on coarse or fine fiber scavengers. A rough calculation, based on the formula for visual range in a fog (Podzimek, 1981)

$$L = \frac{\ln\left(\frac{1}{\epsilon}\right)}{\frac{\pi}{4} n \int_0^{\infty} n_p(d_p)^2 K_{\text{ext}}\left(\frac{\pi d_p}{\lambda}, m\right) d(d_p)} \quad (10)$$

with  $\epsilon = 0.02$ ,  $K_{\text{ext}} = 2.0$ ,  $n$  (total particle concentration)  $\approx 500,000 \text{ cm}^{-3}$  and particle size distribution  $n_p(d_p)$ , leads to  $L$  of

the order of 10 cm. This is consistent with the observation in the smoke chamber. An improvement of visual range by a factor of 1.3 or 1.4 seems to be feasible if a sufficient number of highly effective scavengers will be used. For instance, from the laboratory studies with coarse fiber scavengers (0.5" x 0.5") the scavenger surface density of 0.5 sc./cm<sup>2</sup> would mean a 35.8% improvement in visual range. The evaluation of electron micrographs of particles deposited on coarse and fine fiber scavengers falling in the smoke chamber reveals that the fine fibers collect mainly particles smaller than 0.5 μm, whereas coarse fibers capture also micron size particles. This supports the investigation made in a wind tunnel mentioned earlier. The dual character of smoke particle deposition on coarse fibers is demonstrated in Fig. 12. It was also observed that TiCl<sub>4</sub> smoke particles deposited on the obverse side of the fiber around the stagnation point (line) form chain-like aggregates probably due to the combined effect of electrostatic and inertial force.

The experiments in a cylindrical smoke chamber showed also the importance of investigating the effect of hydrodynamic interaction and dispersion of a large quantity of scavengers released simultaneously. The scavengers dispersed from a point form a cone the shape of which--besides other parameters--depends on the induced air circulation in a specific experimental space. For this reason comparative measurements with the same type of scavengers have been made simultaneously in the smoke chamber (0.8 m<sup>3</sup> volume, 1.6 m high) and in the UMR gymnasium. There a known quantity of scavengers was dropped at a height of approximately 10 m and the scavenger position on the floor was evaluated in reference to the center line of the "dispersion" cone.

The main results of this investigation are summarized in Table I, where the following parameters are calculated: The mean scavenger velocity, standard deviation of deposited scavengers from the cone axis, mean "radius" of circle within which were found 50% of the total number of scavengers and the coefficient of scavenger dispersion. One can observe a permanent difference between the parameters calculated in the chamber and in the gymnasium. In the first case the scavenger settling path was approximately 1.6 m and in the second one 10 m. Settling velocities for the same type of scavengers are higher in the tank than in the gymnasium. To this is related the scavenger dispersion on the floor and the mean "radius" of the circle circumscribed to the area where 50% of scavengers are deposited,  $\bar{r}$ . For the height of the dropping point H, for the coefficient of scavenger dispersion,  $D_S$ , and scavenger settling velocity,  $V_S$ , the  $\bar{r}$  was calculated from the relationship,

$$\bar{r} = (2D_S t)^{1/2} (H \cdot D_S)^{1/2} V_S^{-1/2} \quad (11)$$

Practically all data indicate larger mean radii,  $\bar{r}$ , and dispersion coefficients,  $D_S$ , in the gymnasium. The explanation might be related to a minimum path length along which the steady

scavenger motion will develop and the strong effect of induced air velocities in the smoke chamber. The dispersion coefficient was found to be very large in cases where the shape of scavengers supported their sliding or rotation along their settling path (e.g., paper disks and rectangles in Figs. 14 and 15) in comparison to steady settling of mesh type scavengers in calm air (Fig. 16). Each "Distance Zone" in Figs. 14, 15 and 16 is a multiple of 27.4 cm.

TABLE I  
COMPARISON  
OF SCAVENGER DISPERSION PARAMETERS

SCAVEN. TYPE	FALL VELOCITY [cm/s]		STAND. DEV.		50% RADIUS [cm]		COEFF. DIFFUSION	
	TANK	GYMN	TANK	GYMN	TANK	GYMN	TANK	GYMN
Coarse rect. "dust magn."	191.81	163.66	15.59	4.79	12.122	43.293	68.92	159.63
Small coarse rect. "dust magnet"	192.81	166.35	15.89	4.79	12.293	33.790	70.87	98.84
Coarse fine fiber "dust magnet"	176.35	173.40	8.79	10.78	33.000		97.97	
Small fine fiber "dust magnet"	146.05 146.05 146.05	120.90	18.29 18.29 18.29	10.78	19.308 14.529 15.52	45.755	133.13 75.38	129.15
Paper disc r=0.6 cm	150.76	143.35	9.40	10.17	33.840	197.28	516.10	2892.80
Paper rectang. 0.13x0.3 cm	177.31 177.31 177.31	175.70	15.96 15.96 15.96	11.95	34.837 36.542 33.626	130.565	526.11 578.87 490.191	1559.36
Paper square 0.13x0.3 cm	177.31 177.31 177.31	173.93 175.70	15.96 15.96 15.96	14.976 11.95	34.837 36.542 33.626	47.843 130.565	526.11 578.87 490.191	207.36 1559.36
Paper square 0.13x0.14 cm		173.93		14.976		47.843		207.36

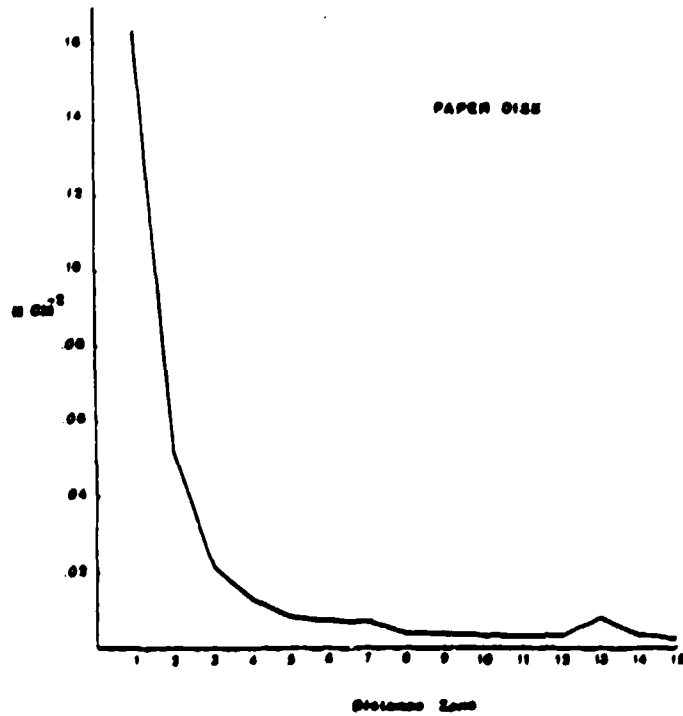


Fig. 14 Number of deposited circular punch cards ( $d = 0.66$  cm) in dependence on the distance from the vertical. The scavengers were dropped from the plateau 9.60 m above the floor.

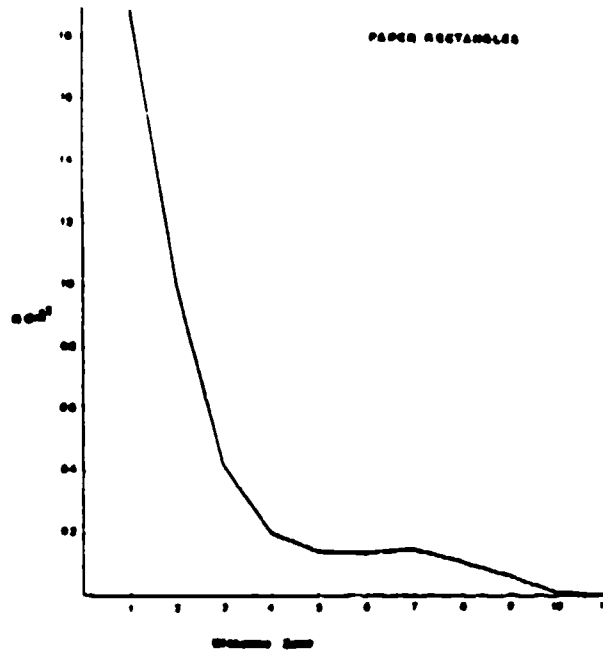


Fig. 15 Number of deposited paper rectangles (0.13 x 0.3 cm) in dependence on the distance from the vertical. Each circular zone width on the floor is 27.4 cm. The scavengers were dropped from the plateau 9.60 m above the floor.

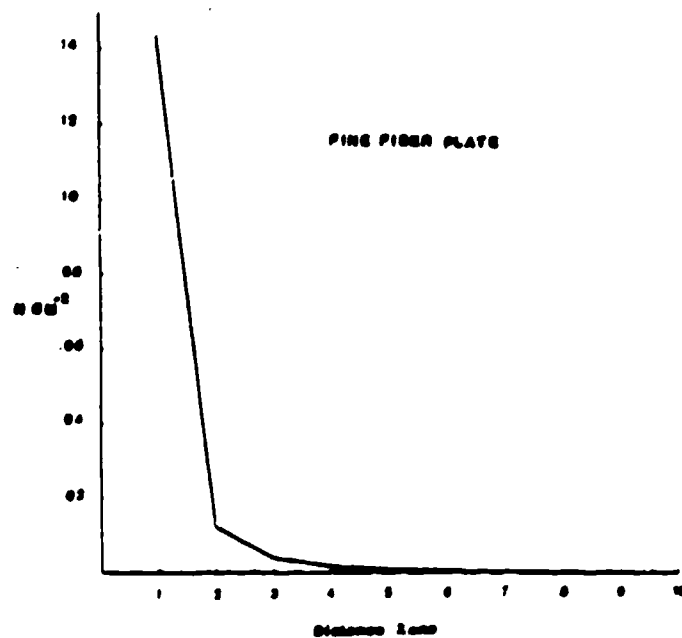


Fig. 16 Number of deposited fine fiber plates (1.25 cm x 1.25 cm x 0.6 cm) in dependence on the distance from the vertical. Each circular zone width on the floor is 27.4 cm. The dropping plateau was 9.60 m above the floor.

#### 4. INVESTIGATION OF THE FALLING SCAVENGER ZONE

A large quantity of scavengers induces downdrafts inside a scavenger zone. These downdrafts and related horizontal air motion affect the scavenger collection efficiency and motion, and potentially, the transport of smoke particles towards the ground.

During the past three years the two-dimensional model, which in the first stage does not include the thermal instability terms, was developed (Podzimek, 1983; Podzimek and Smith, 1986). The model is suitable for investigation of the impact of different scavenger mixing ratios (concentrations), isotropic turbulent exchange coefficient and release height on the evolution of the scavenger cloud. Recently the model was extended to include the effect of slight horizontal wind on scavenger dispersion and induced air motion. The basic set of equations with the boundary and initial conditions is described in Appendix E.

Summarizing the results of the investigation of the evolution of the falling scavenger zone with its potential impact on the smoke particulate transport to the ground, one finds the two-dimensional model suitable for describing the role of the main parameters affecting the zone dynamics. Apparently the most important parameter is the scavenger mixing ratio (g sc./g air). For non-spherical scavengers it would be necessary to introduce an "effective mixing ratio" which will account for the aerodynamic effect of non-spherical collectors. The change of mixing ratio from 0.01 g sc./g air to 0.04 g sc./g air is directly proportional to the speeding up of the scavenger dispersion through the calm atmosphere (Fig. 17). The lowest position of the zone,  $z$ , and the maximum width,  $x$ , for both mixing ratios are plotted in Fig. 18 as a function of time. The dispersing cloud generates further the induced motion downwards (velocity component,  $w$  in Fig. 19) and entrains the air from outside with the horizontal component,  $u$  (in Fig. 20). In this case scavengers were dropped at 2 km altitude and were settling with the fall velocity of  $1.5 \text{ m s}^{-1}$ . The most intense downdraft developed after 300 seconds and when the scavenger zone (of original dimensions 400 m x 400 m) reached the ground the induced velocity surpassed 13% of that of the scavengers. Very interesting is also the pattern of horizontal velocity isolines (Fig. 20) which demonstrates the intense entrainment of the air when scavenger zone is close to the ground. This air mass exchange contributes also to the increasing visibility at the ground. The transport of smoke particles downwards is accompanied, however, by the decreasing efficiency of inertial deposition of larger smoke particulates on the scavengers, because the collection efficiency is proportional to the velocity difference between the scavenger and aerosol.

The value of turbulent exchange coefficient does not affect much the air motion around and inside of the falling scavenger zone. Decisive for the induced air motion is the time available for the full evolution of the air circulation and the initial shape of the scavenger zone. The following combinations of the horizontal and vertical dimensions of the scavenger zone have been used: 800 m x 200 m; 500 m x 320 m; 400 m x 400 m and 320 m

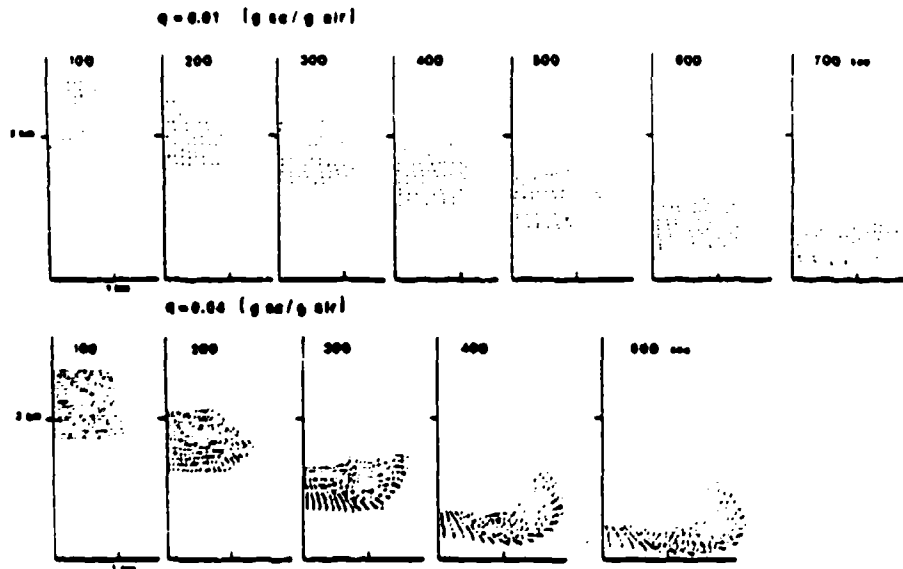


Fig. 17 Evolution of falling scavenger zone with  $\rho = 0.01$  and  $0.04$  g sc./g air and  $V = 1.5$  m/s,  $K_t = 1000$  m<sup>2</sup>/s.

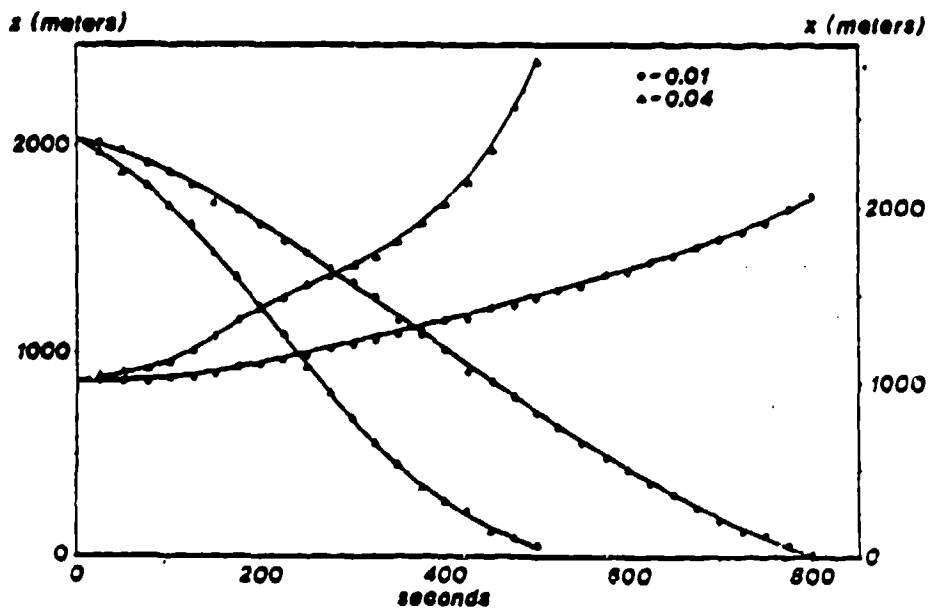


Fig. 18 The mean heights,  $z$ , of the falling scavengers front and the maximal widths,  $b_{\max} = x$ , as a function of time for  $g = 0.001$  and  $0.04$  g sc./g air. Other parameters are the same like in Fig. 17.

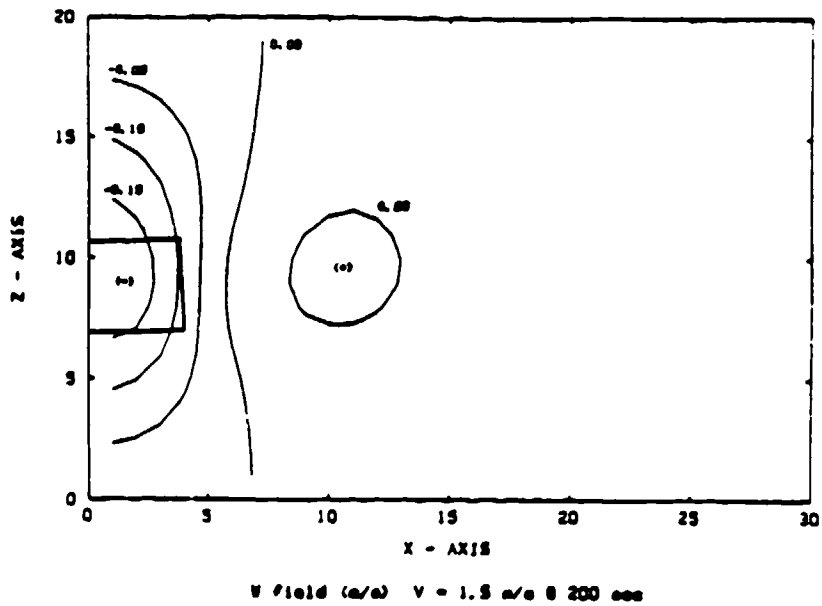


Fig. 19a

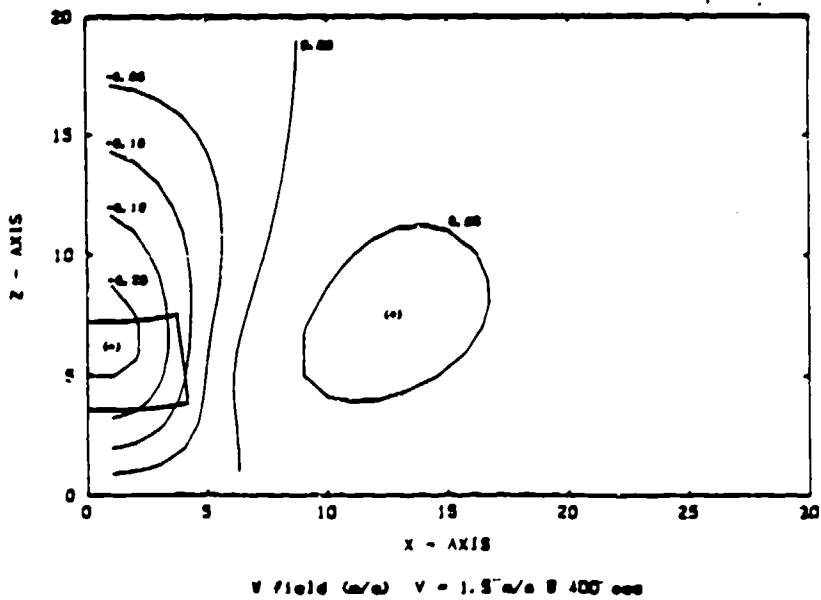


Fig. 19b

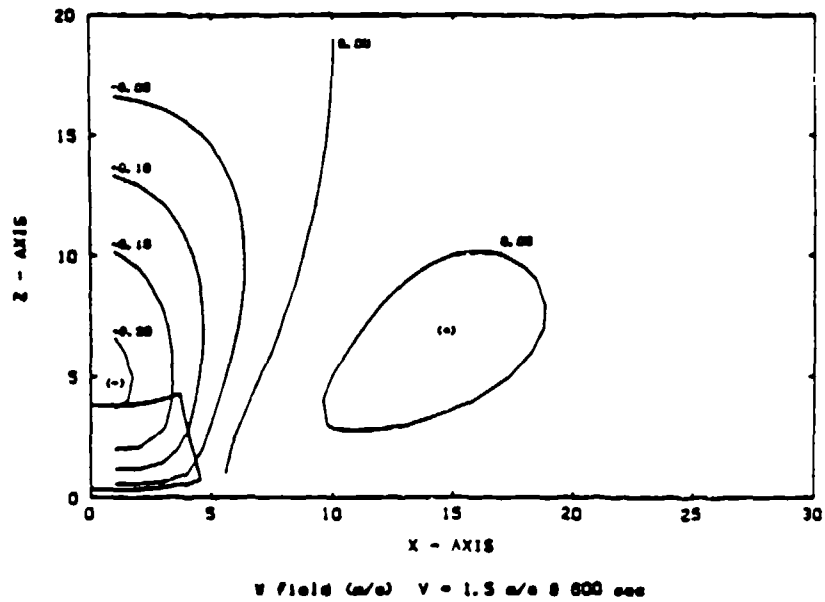


Fig. 19a,b,c Impact of the 400 x 400 m falling scavenger zone on the induced w - velocity components.

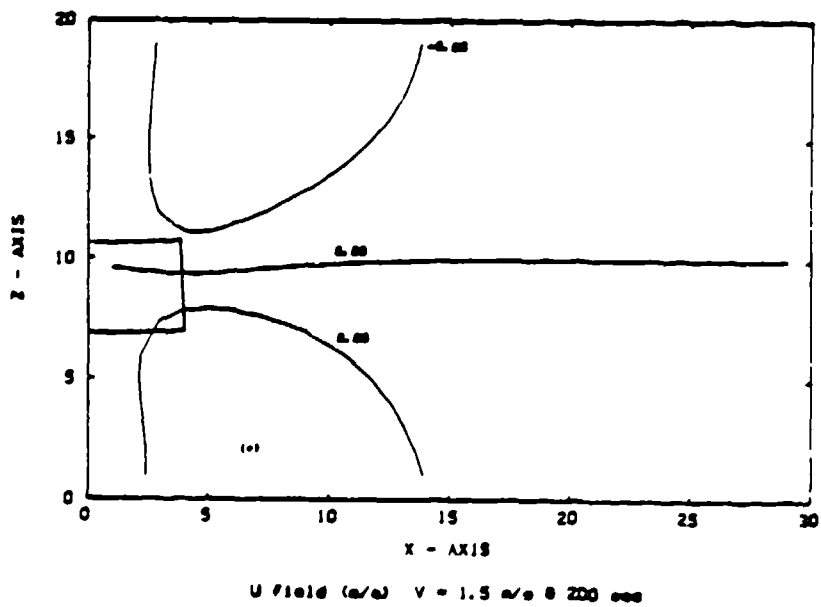
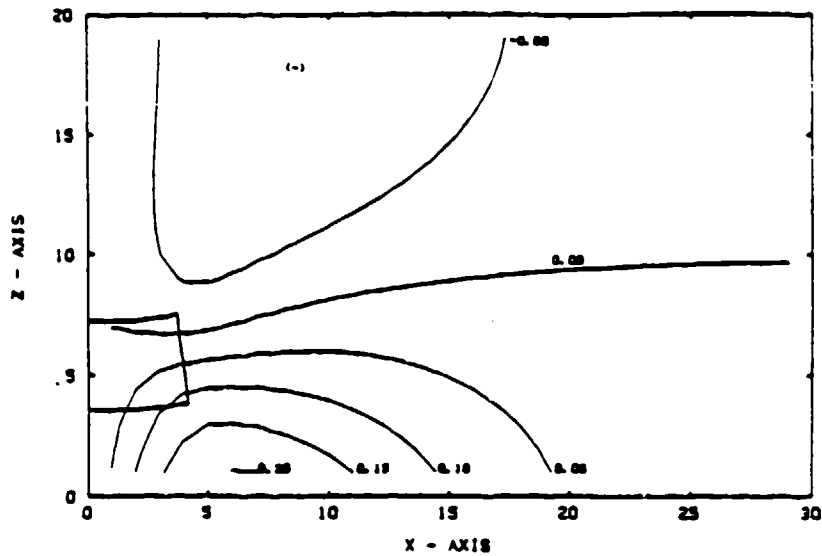
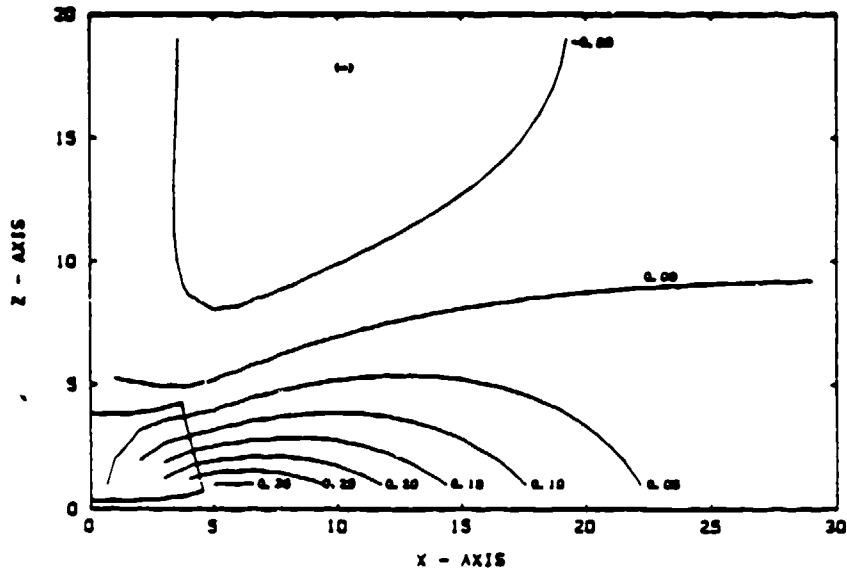


Fig. 20a



U field (m/s) V = 1.5 m/s @ 400 m/s

Fig. 20b

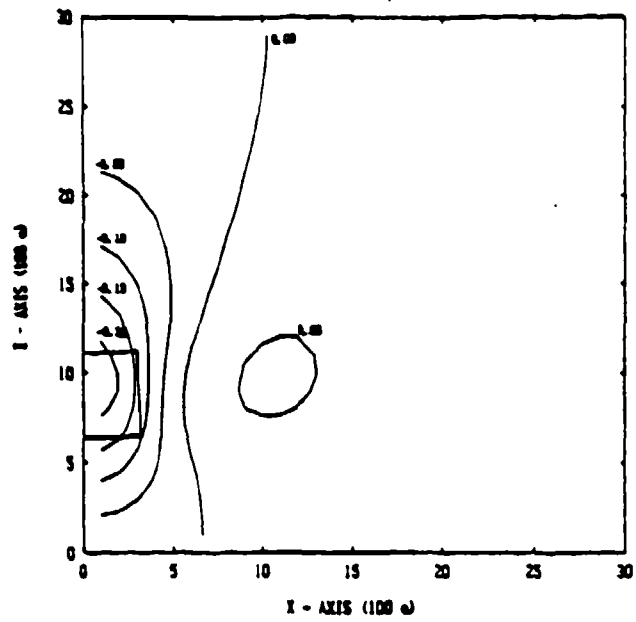


U field (m/s) V = 1.5 m/s @ 600 m/s

Fig. 20a,b,c Impact of the 400 x 400 m falling scavenger zone on the induced u - velocity component.

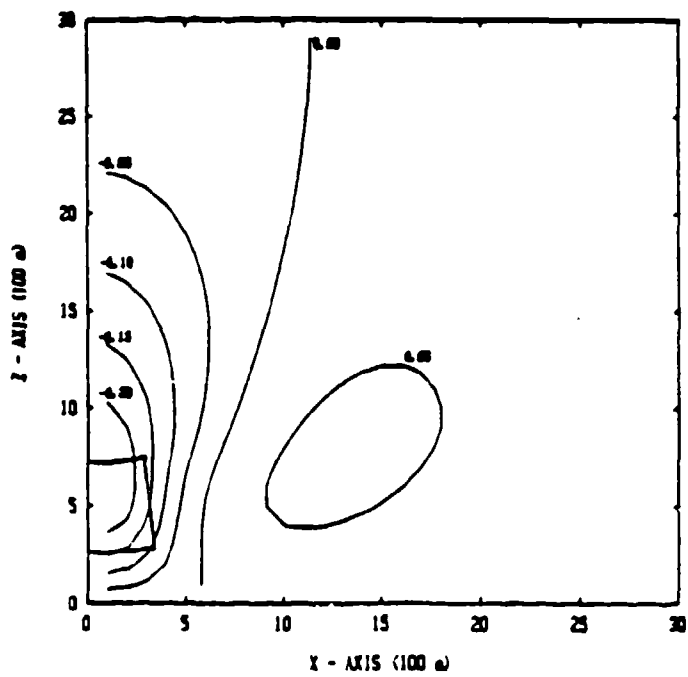
x 500 m. The most significant effect have thick zones (320 m x 500 m, 400 m x 500 m) which--for scavenger settling velocity of  $V_s = 1.73 \text{ m s}^{-1}$ --induced downdrafts surpassing  $0.2 \text{ m s}^{-1}$  (Fig. 21). Induced downdrafts by thin zones (800 m x 200 m) of scavengers released initially at an altitude of 1.5 km induced velocities at the ground only slightly overriding  $0.1 \text{ m s}^{-1}$  (Fig. 22).

The numerical modeling of the evolution of the falling scavenger zone at slight side winds concentrated mainly on "spherical" scavengers dispersed at a high altitude (7 km). Their settling has been accompanied by induced downdrafts and considerable deformation of the zone due to the effect of horizontal velocity ( $u = 1 \text{ m s}^{-1}$ ) constant in the whole field. The model with boundary conditions outlined in the Appendix E can be applied to other velocity profiles and to the changing air density with altitude. The dramatic evolution of the scavenger cloud after a long time of settling (Fig. 23) indicates the necessity of investigating the scavenger dispersion at several typical situations in the troposphere and in the planetary boundary layer (e.g., stable and unstable thermal stratification) if larger areas are intended to be covered by scavengers.



V field (m/s)  $V = 1.73 \text{ m/s} @ 200 \text{ mm}$

Fig. 21a



V field (m/s)  $V = 1.73 \text{ m/s} @ 400 \text{ mm. (320 \times 500 \text{ m.})}$

Fig. 21b

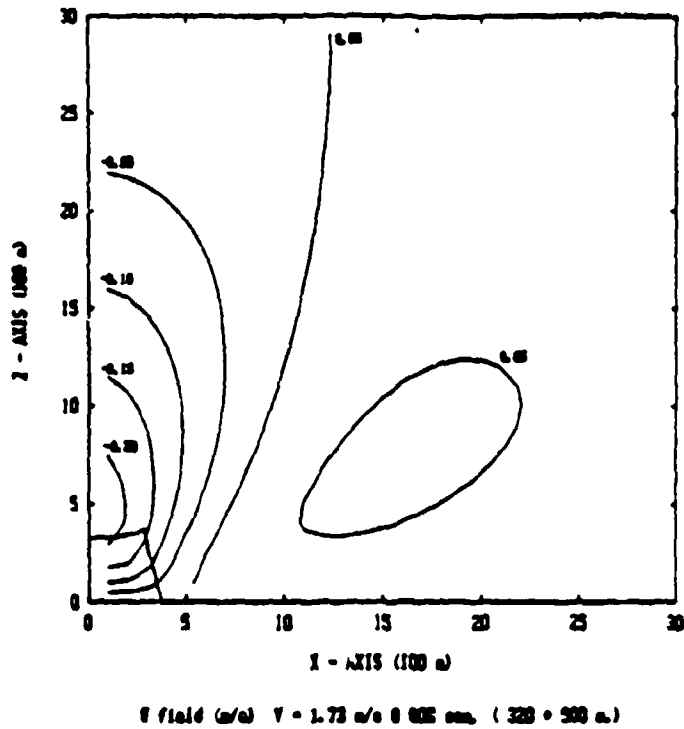


Fig. 21a,b,c Impact of the initial shape of the zone (320 m x 500 m) on the zone evolution. Calculated for  $q = 0.01 \text{ g sc./g air}$ ,  $H_R = 1 \text{ km}$ ,  $V_S = 1.73 \text{ m/s}$ ,  $K_t = 1000 \text{ m}^2/\text{s}$ .

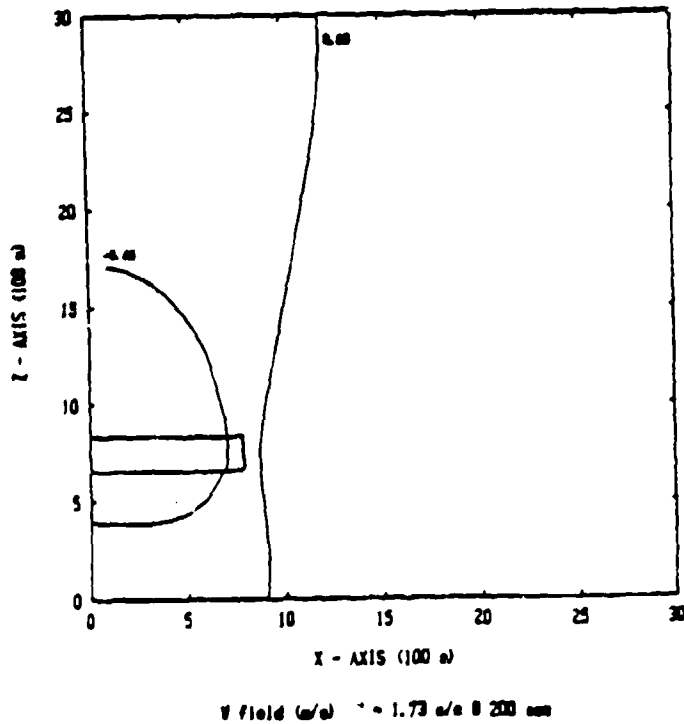
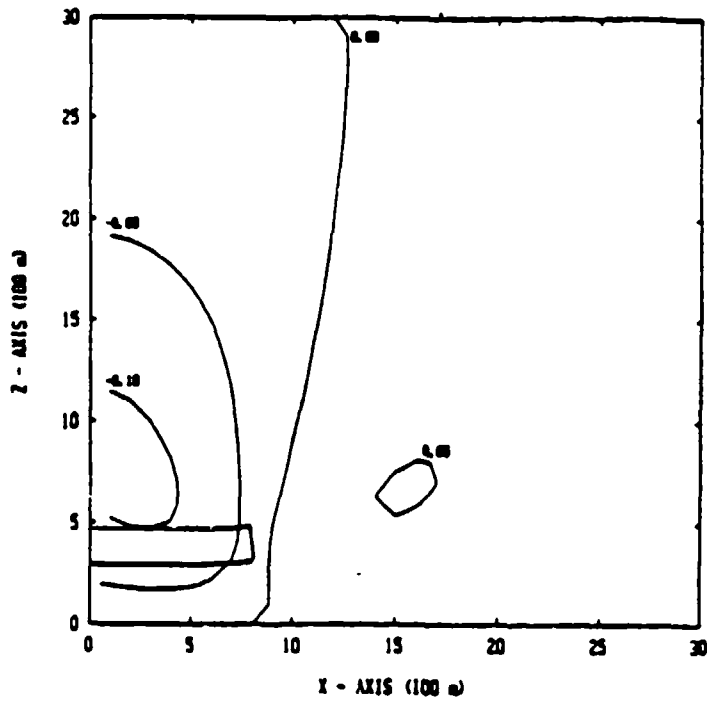
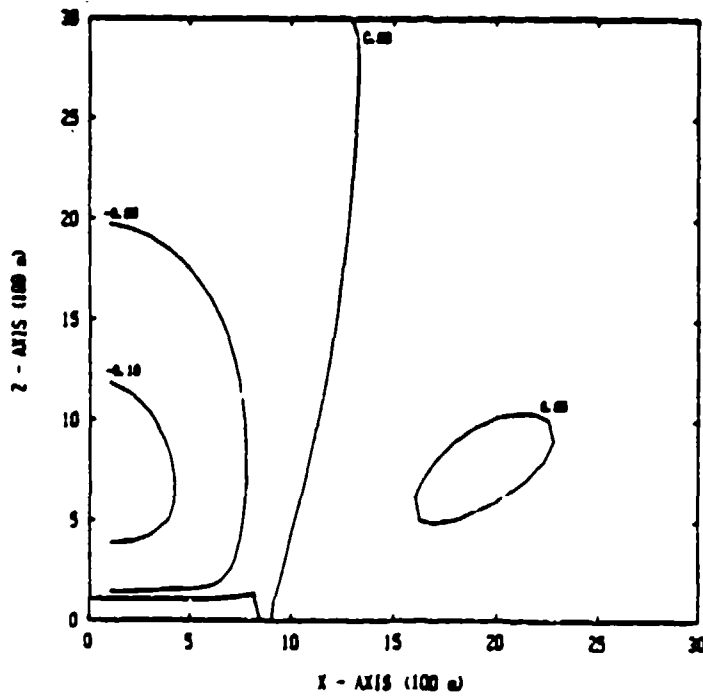


Fig. 22a



V field (m/s)  $V = 1.73$  m/s @ 400 sec

Fig. 22b



V field (m/s)  $V = 1.73$  m/s @ 800 sec

Fig. 22a,b,c Impact of the initial shape of the zone (800 m x 200 m) on the zone evolution. Calculated for  $q = 0.01$  g sc./g air,  $H_R = 1$  km,  $V_S = 1.73$  m/s,  $K_t = 1000$  m<sup>2</sup>s.

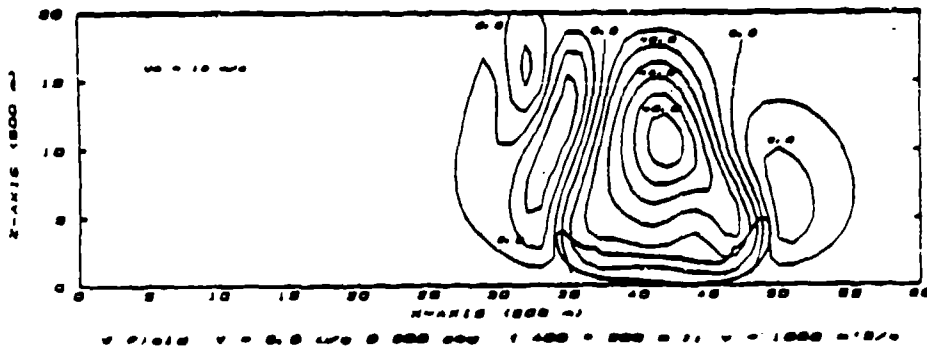
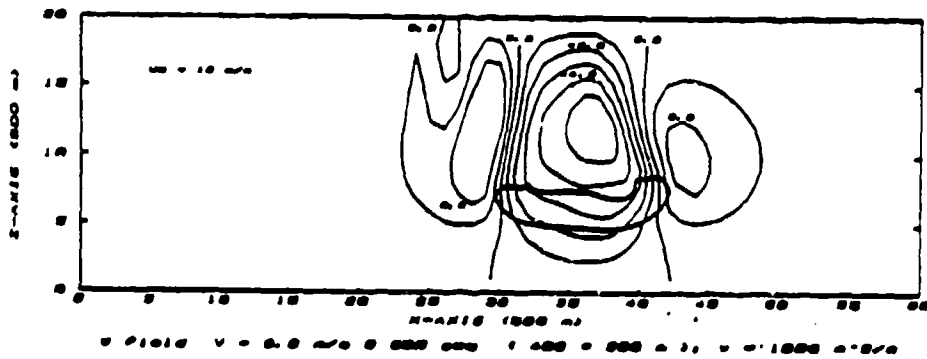
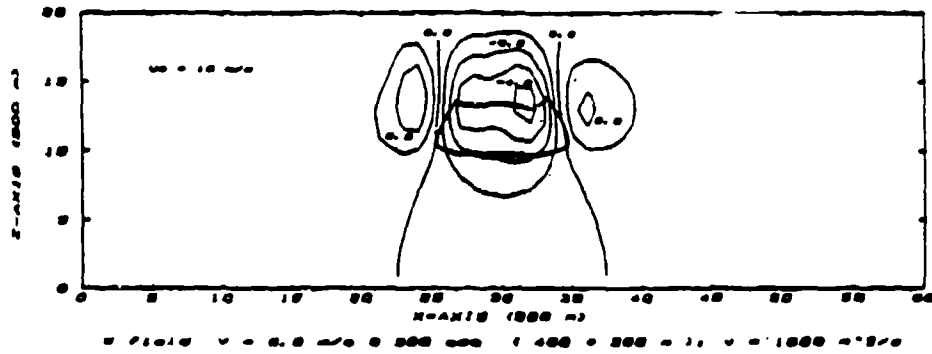


Fig. 23a,b,c Falling scavenger zone evolution at a horizontal wind 1.0 m/s.

Blank

## 5. DISCUSSION OF THE MAIN RESULTS

The main goal of this project was to determine the feasibility and effectiveness of a scavenging operation for improving visibility in a military smoke cloud. The previous investigations indicated higher scavenging efficiency of nonspherical collectors for smoke aerosols with particle sizes from 0.2  $\mu\text{m}$  to several  $\mu\text{m}$ . Different shapes of scavengers (disks, squares, rectangles) and their motion do not have a decisive impact on collection efficiency which rarely surpassed 1% for a disk and  $Re$  up to 20 according to numerical models (Podzimek, 1981). Experimental data were almost one order of magnitude smaller than the theoretical values for smoke particle radii around 0.3  $\mu\text{m}$ . Collection efficiencies of electrically charged disks varied between 3% and 10%, however, the problem of how to maintain the high electric charge on collectors during small scale experiments remained unresolved. Finally, it was found that for smoke particle sizes within the "Greenfield gap" the most effective scavengers are mesh or grid type models, mainly if "self-charging" electrete type materials are used. Concerning the hydrodynamic interaction of a population of scavengers falling simultaneously in the "Falling Scavenger Zone" was recommended to follow closely the zone evolution in the future with regard to the results included. In this report we would like to call attention to the new findings made during the past three years and to the results obtained while using improved equipment or numerical models. Also, we would like to address the question of practical applicability of our study for medium or large scale experiments in the field.

Collection efficiency of thin oblate spheroids was extended to  $Re = 80$ . At  $Re$  higher than 80 our numerical model--which is based on creeping flow equations--failed to yield reasonable results. Still remains to explain the shape of the collection efficiency curve for  $0.1 \leq Re \leq 5.0$ . In this transitional region starts to develop the instability on the reverse side of a disk which has an impact on particle deposition through phoretic forces. The additivity of the diffusion and phoretic forces was questioned by Carstens and Martin (1982), however, it can be assumed that the effect of these forces will be smaller in a smoke cloud than in water droplet or in a mixed cloud (Podzimek, 1984).

The study of particulate deposition on cylinders was intended to confront some of our results of wind tunnel measurements with a simple theory of deposition on a single fiber or a pair of hydrodynamically interacting fibers. Compared to the known solutions of particulate deposition in the potential flow (Albrecht 1931; Sell 1931; Glauert, 1940; Langmuir and Blodgett, 1946; Davies and Peetz, 1955) the presented solution might be more accurate and very close to the results of the Davies and Peetz study. It can also be used for the study of particle deposition on two cylinders close together and yield quite satisfactory results for large Stokes numbers of particulates (sizes larger than 1  $\mu\text{m}$  and densities  $\geq 2.0 \text{ g cm}^{-3}$ ). For these conditions the particle deposition rate might be close to the deposition in viscous flow solved in a numerical

model by Schlamp (1977). His model deduced for the deposition of cloud droplets on columnar ice crystals was available to our group. It was applied to the deposition of smoke particulates smaller than cloud droplets in our group with mixed success.

After we became familiar with the Brown's multi-fiber model (Brown, 1983) which is described in Appendix D we tried to use it for particle deposition on parallel or staggered fiber array. In our opinion, the model has to be improved in order to describe in a more realistic way the conditions inside a filter type scavenger. On the other side, it has great potential if applied to our grid type scavengers or thin not very dense packed filter type scavengers.

This study supports the conclusion from the previous report that the effect of an electric charge is significant. The only Coulomb force interaction is, however, an oversimplification of the whole process. The new calculation supports also the previous conclusion that the collection efficiency is lower for particle radii larger than  $5.0 \mu\text{m}$  if compared to the uncharged collector. We might speculate about the neglected effect of image forces. Finally, the discrepancy between the calculated and measured values of collision efficiency (Fig. 2) might be explained by the fact that the model assumes a single first collision of the smoke particle. The second and all following particles are impacting the collector as if the preceding collisions would not happen or if the aerodynamic and electrostatic field around the collector would remain the same. Conclusions similar to those made for thin oblate spheroid bearing an electrostatic charge can be made for a cylinder (Podzimek and Martin, 1984).

Comparing the theoretical results of particle deposition of collectors of simple geometry (disks, cylinders) with the wind tunnel measurements or with the observed deposition of particulates on scavengers falling in a smoke chamber we observe usually smaller deposition on exposed scavengers. The explanation might be due to the imperfect modeling of particulate behavior in the boundary layer (particle rotation in a velocity gradient, wake effect). Considerable part of particulates might rebound from the collectors surface. The last hypothesis is supported by the fact that charged collectors showed a deposition comparable with theoretical results. The main discrepancy might be, however, explained by the used technique of deposited particle counting on the collectors surface. Usually the smoke particles are piled up or make some larger aggregates--which in principle will increase the collection efficiency--but it is very difficult to count all particles in the electron micrographs. Many of the small particles will not be seen in the proximity or under the large ones. Several of the trials to check the reproducibility of the particle counting led to the conclusion that the mean errors of counting might override  $\pm 30\%$  of the counted value.

One of the most significant results of the experiments seems to be the high smoke particle deposition on the reverse side of scavengers. In the case of a disk it might be comparable to the deposition on the obverse side which, unfortunately, cannot be

described by numerical models at  $Re > 10$  (for a disk). The scavenger motion or oscillation will not effect significantly the deposition of particulates on scavengers considered in this report.

The experiments in cylindrical smoke chamber were marked by a large scatter of data from the measurement of the light extinction after the scavengers were dropped in a dense  $TiCl_4$  smoke. The arrangement of the experiment was the same like that described in our previous report (Podzimek, 1981). More emphasis was put, however, on the reproducibility of the measurements. The generation of  $TiCl_4$  aerosol was controlled within approximately  $\pm 20\%$  of deviation of the individual points on the size distribution curve during the total duration of the experiment (usually more than 1 hour). The large fluctuation of signals in the past was explained by the different mode of scavenger dropping (frequency and initial position of scavengers) and the low probability of hitting the sensitive volume of the light beam. Further was observed that large quantity of scavengers dropped at the same time did not cause a markable change in light extinction. This is explained by the induced downdraft in the relatively small smoke chamber. It is hypothesized that the downdraft is reducing the velocity difference between smoke particle and scavenger, and in this way, also the collection efficiency of scavengers will be smaller.

The observation of scavenger interaction and formation of a dispersing cone in the smoke chamber 1.6 m high led to the question of how to transfer the data from the chamber into the real atmosphere. Experiments in the UMR gymnasium showed clearly that the difference in the dispersion angle depends on scavenger type, size (mass) and motion, but also on the rate of scavenger dropping. Scavengers required a certain time (several seconds) for forming a steady dispersing cone in spite of the fact that their relaxation time for resuming a steady motion (of a single scavenger) is of the order of tenths of a second. We believe, that the observed dispersion cones or coefficients of scavenger dispersion in the calm atmosphere are useful parameters for practical use in the field. The data were also used for estimating the overall effect of SPADES technique for clearing a military smoke cloud. A logical continuation of this study ought to be the experiments with the most effective (electrete grid or filter type) scavengers at a slight side wind in the atmosphere or in an aerodynamic wind tunnel of large cross section.

The methodology of a successful application of scavenger technique for clearing of a smoke cloud has to be combined with an assessment of the clearing effect through induced downdrafts. With regard to the dispersion of scavengers from a helicopter, airplane, or parachute the 2-D model simulating the effect of a "line source" seems to be an appropriate approximation. Its extension for simulating the scavenger dispersion at a slight side wind and for atmosphere with variable air density has been already done. Especially the study of the effect of  $1 \text{ ms}^{-1}$  horizontal wind is an important contribution to the study of clearing polluted atmospheric boundary layer by artificial or natural (rain drops, ice crystals) scavengers. The further

evolution of this model could go via inclusion of the thermal stratification of the atmosphere (similar study with different goals has been made by Girard and List, 1975) and application of a specific wind velocity profile in the boundary layer.

Scavenger mixing ratio seems to be one of the most important parameters directly related to the generated downdrafts. This leads to a logical conclusion that for an effective clearing of smoke cloud have to be combined: That collecting the particles on special type of scavengers and that supporting their transport towards the ground. The second technique would not require the use of any type of effective scavengers and the positive effect could be obtained by dispersing dry ice grains, water droplets, or provoking artificial rain over the area at favorable meteorological situation. Other important parameters for inducing an effective downdraft are the settling velocity of scavengers, the minimum time required for downdraft evolution and the initial thickness of the scavenger zone. They can be easily controlled during medium or large scale experiments.

In compliance with point 4 of part "8. Identification of the Main Goals" in our proposal to the program DAAK-11-83--which we intended "to establish a solid basis for the application of scavenging technique in the field..." we tried to quantify the impact of the main factors contributing to the evolution of downdrafts in the falling scavenger zone. These factors depend also on the applied technology of scavenger dispersion: Several scenarios were suggested for electrete fiber dispersion from an airplane, helicopter or a parachute. Three groups of four senior students studied (without knowing the details about the program DAAK-11-83) the technology of scavenger release and dispersion. The reports--available in our office include the details on the scavenger generators, estimates of generators output and the amount of scavengers necessary for 30% improvement of visibility at the ground. These numbers (in Table II) are based on the measured data in the wind tunnel and in the smoke chamber and do not include the effect of induced downdrafts.

Particle removal efficiencies in Table II represent the most conservative numbers which were deduced from a model (Podzimek, 1979) and wind tunnel measurements with single fibers. The effect of fiber crossing in the mesh--which might enhance the collection efficiency--is not considered.

The total effect would be certainly more favorable depending on the choice of scavengers for the most effective downdraft. Heavy scavengers with compact structure will be more suitable for a thin layer of smoke in reference to downdraft generation. Apparently the combination of different techniques during one action will be the most appropriate way for clearing a military smoke cloud in our opinion.

TABLE II

TOTAL WEIGHT OF SCAVENGERS NECESSARY FOR IMPROVING  
THE VISUAL RANGE OF 30% OVER AN AREA OF 100 m x  
100 m IN TiO<sub>2</sub> SMOKE

Scavenger Type size [cm]	Scav. Weight [g]	Particle Removal Efficiency in % for particle radii [ $\mu$ m]					Weight of Scavengers [kg]
		<0.25	0.50	0.75	1.00	1.25	
Small coarse fiber 1.3 x 1.3 x 0.024	0.023	4.7	3.2	1.1	0.9	0.3	815.0
Large coarse fiber 3.1 x 3.1 x 0.024	0.125	4.7	3.2	1.1	0.9	0.3	1,632.0
Thin fine fiber 1.8 x 1.8 x 0.7	0.031	7.1	2.3	7.5	3.2	0.6	600.0
Thick fine fiber 1.8 x 1.8 x 1.4	0.058	7.1	2.3	7.5	3.2	0.6	756.0

## 6. CONCLUSION

The program of three year effort was formulated in our proposal in paragraph "7. Time Schedule" and in "8. Identification of the Main Goals". All points of our program were followed in accordance with our proposal, however, with different intensity. For example, interaction of diffusional and phoretic forces was not followed in much detail when it was clear that diffusion and diffusiophoresis will not play a major role in smoke particle ( $0.1 < r_p < 5.0 \mu\text{m}$ ) deposition on insoluble fibers. Also the effect of oscillating scavengers had an orientational character due to the little effect of the observed frequencies and scavenger motion amplitudes on the collection efficiency of planar scavengers.

Most effective were the grid type scavengers and filter type scavengers, especially those made of electrete fibers. The physical mechanism of their action is not completely known, however, their collection efficiencies (referred to the ideal cylinder type fiber) will surpass 10%. This finding, based mainly on the wind tunnel experiments, seems to be supported also by the results from the smoke chamber. In the future attention should be paid to the appropriate combination of fibers with different geometry and composition in order to reach a maximal effect in polydisperse smoke particle removal.

For medium and large scale experiments in the field the knowledge of dispersion characteristics of a large population of falling scavengers seems to be of utmost importance. Experiments in large scale (10 m settling path) showed clearly that each type of scavengers needs a specific time for developing the "typical" shape of a dispersion cone and that the experiments in small smoke chambers must be corrected.

During the study of direct scavenging of particulates was discovered that the air downdraft induced in the falling scavenger zone might be another factor contributing to the effective transport of smoke particles to the ground. The magnitude of the downdraft depends on the scavenger mixing ratio and settling velocity. The time required for the fully developed downdraft (surpassing often 10% of scavenger settling velocity) and the initial thickness of scavenger zone are other important parameters determining the evolution of induced air circulation and transport of smoke particles to the ground. The appropriate combination of direct scavenging with the induced downdraft technique--which can be accomplished by simple water droplet dispersion or cloud seeding--might be an effective technique especially for smoke clouds formed during very stable thermal stratification in the atmospheric boundary layer.

## REFERENCES

- Albrecht, F., 1931, Theoretische Untersuchungen uber die Ablagerung von Staub aus stromender Luft und ihre Anwendung auf die Theorie der Staubfilter, Phys. Z. 32, 48.
- Bergun, N.R., 1951, A method for numerically calculating the area and distribution of water impingement on the leading edge of an airfoil in a cloud, National Advisory Committee for Aeronautics, Tech. Note 2476.
- Brown, R.C., 1984, Many-fiber model of airflow through a fibrous filter, J. Aerosol Sci., 15, 583-593.
- Carstens, J.C., and J.J. Martin, 1982, In-cloud scavenging by thermophoresis, diffusiophoresis, and Brownian diffusion, J. Atmos. Sci., 39, 1124-1129.
- Clark, T.L., and R. List, 1971, Dynamics of a falling particle zone, J. Atmos. Sci., 28, 718-727.
- Davies, C.N., and C.V. Peetz, 1955, Impingement of particles on a tranverse cylinder, Proc. R. Soc. A. 234, 269-295.
- Frankel, S.P., 1950, Convergence rates of iterative treatments of partial differential equations, Math. Tables and Other Aids to Computation, Vol. 4, 65-75.
- Girard, C., and List, R., 1975, Thermodynamics of falling precipitation zones, Pageoph., 113, 1035-1053.
- Glauert, M., 1940, Rep. Dep. Sci. Industr. Res., Lond., no. 4805, D.W.T.7.
- Happel, J., 1959, Viscous flow relative to arrays of cylinders, Am. Inst. Chem. Eng. J., 5, 174-177.
- Kirsch, A.A., and N.A. Fuchs, 1967, Studies on fibrous aerosol filters - II. Pressure drops in systems of parallel cylinders, Ann. Occup. Hyg., 10, 23-30.
- Kuwabara, S., 1959, The forces experienced by randomly distributed parallel circular cylinders spheres in viscous flow at small Reynolds numbers, J. Phys. Soc., Japan, 14(4), 527-532.
- Langmuir, I., and K.B. Blodgett, 1946, A mathematical investigation of water droplet trajectories, Tech. Service Command, Army Air Forces Tech. Rep. No. 5418, Dayton, Ohio.
- Liu, Yih-Jong, 1935, Deposition of micron and submicron particulates on cylinder-contribution to the theory of filtration, M.S. Thesis: University of Missouri-Rolla.

Martin, J.J., K.P. Wang, and H.R. Pruppacher, 1980a, On the efficiency with which aerosol particles of radius larger than 0.1  $\mu\text{m}$  are collected by simple ice crystal plates, Pure Appl. Geophys. 118, 1109-1129.

Martin, J.J., K.P. Wang, and H.R. Pruppacher, 1980b, A theoretical determination of the efficiency with which aerosol particles are collected by simple ice crystal plates, J. Atmos. Sci., 37, 1628-1938.

Martin, J.J., K.P. Wang, and H.R. Pruppacher, 1980c, A theoretical study of the effect of electric charges on the efficiency with which aerosol particles are collected by ice crystal plates, J. Coll. Interf. Sci., 78, 44-56.

Martin, J.J., P.K. Wang, and H.R. Pruppacher, 1981, A numerical study of the effect of electric charges on the efficiency with which planar ice crystals collect supercooled cloud drops, J. Atmos. Sci., 38, 2462-2469.

Martin, J.J., and J. Podzimek, 1982, Scavenging of smoke particles by planar collectors, Proc. CSL Conf. on Obscuration and Aerosol Research, Aberdeen, August, 99-112.

Pitter, R.L., 1977, Scavenging efficiency of electrostatically charged thin ice plates and spherical aerosol particles, J. Atmos. Sci., 34, 1797-1800.

Pitter, R.L., and H.R. Pruppacher, 1974, A numerical investigation of collision efficiencies of simple ice plates colliding with supercooled water drops, J. Atmos. Sci., 31, 551-559.

Podzimek, J., 1979, Survey of techniques for clearing military smoke clouds, USAARADCOM, Aberdeen Proving Ground.

Podzimek, J., 1981, Clearing of military smoke cloud with scavenging techniques, Final Rep. DAAG-79-C-0073, UMR.

Podzimek, J., 1983, Investigation of a technique clearing/modifying a military smoke cloud, Final Rep. DAAK-11-81-C-0075, UMR.

Podzimek, J., 1984, Prerequisites of a successful modification of a fog or cloud by scavenging techniques, Ext. Abstr. 9th Conf. on Weather Modification, Park City, May, AMS, Boston, 18-19.

Podzimek, J., and J.J. Martin, 1984, Deposition of particulates on charged planar scavengers, Preprint Vol. 7th Int. Conf. on Atmospheric Electricity, Albany, June, AMS, Boston, 57-62.

Podzimek, J., and T. Smith, 1986, Overall effect of scavenger falling zone on clearing a smoke cloud, Proc. CRDEC Sci. Conf. on Obscuration and Aerosol Research, Ed. R. Kohl, Aberdeen.

Roache, P.J., 1982, Computational Fluid Dynamics, Hermosa Publ. Albuquerque, pp. 36-39 and 117-119.

Schlamp, R.J., 1977, A numerical investigation of the efficiency with which simple columnar crystals collide with supercooled water drops, Ph.D. Thesis, UCLA, Los Angeles.

Sell, W., 1931, Z. Ver. deutsch. Ing. p. 295.

Spielman, L., and S.L. Goren, 1968, Model of predicting pressure drop and filtration efficiency in fibrous media, Env. Sci. Techn. 2, 279-287.

Shyu, 1986, Part of the M.S. Thesis (in preparation) UM-Rolla.

Young, D., 1954, Iterative methods for solving partial difference equations of elliptic type, Trans. Amer. Math. Soc., 76, 92-111.

Blank

## APPENDIX A

### CALCULATION OF PARTICLE TRAJECTORIES FOR POTENTIAL FLOW

For sufficiently high  $Re$  the model by Bergrun (1951) (potential flow around a cylinder) and for small  $Re$  the model by Schlamp (viscous flow) was applied. The potential flow assumes that the inertial forces outweigh the frictional forces in particle deposition and--if the effect of boundary layer can be neglected--that a good description of the particle deposition will be obtained for the front side of the cylinder. The actual flow on the reverse side, however, deviates much from reality.

The basic equations for the radial and tangential components of the ideal flow past a cylinder of radius  $R_c$  are (Liu, 1935)

$$v_r = u_\infty \left(1 - \frac{R_c^2}{r^2}\right) \cos \theta \equiv \frac{1}{r} \left(\frac{\partial \psi}{\partial \theta}\right) \quad (1-1)$$

$$v_\theta = u_\infty \left(1 + \frac{R_c^2}{r^2}\right) \sin \theta \equiv - \left(\frac{\partial \psi}{\partial r}\right) \quad (1-2)$$

with the corresponding stream function

$$\psi = u_\infty r \sin \theta \left(1 - \frac{R_c^2}{r^2}\right) . \quad (1-3)$$

From the definition and chain rule follows

$$u_\theta = r d\theta/dt = r(\partial\theta/\partial x)(\partial x/\partial t) + r(\partial\theta/\partial y)(\partial y/\partial t) ; \quad (1-4)$$

$$u_r = dr/dt = (\partial r/\partial x)(\partial x/\partial t) + (\partial r/\partial y)(\partial y/\partial t) . \quad (1-5)$$

From the trigonometric relation

$$\tan \theta = y/x ; \theta = \tan^{-1}(y/x)$$

and

$$r = (x^2 + y^2)^{0.5} ,$$

can be deduced

$$\partial \theta / \partial x = -yx^{-2} / (1 + (y/x)^2) = -y / (x^2 + y^2) ;$$

$$\partial \theta / \partial y = x^{-1} / (1 + (y/x)^2) = x / (x^2 + y^2) ;$$

$$\partial r / \partial x = 0.5(x^2 + y^2)^{-0.5} 2x = x(x^2 + y^2)^{-0.5} ;$$

$$\partial r / \partial y = 0.5(x^2 + y^2)^{-0.5} 2y = y(x^2 + y^2)^{-0.5} .$$

Substituting these equations into equation (1-4) and 1-5), one obtains

$$\begin{aligned} u_{\theta} &= -y(x^2 + y^2)^{-0.5} v_x + x(x^2 + y^2)^{-0.5} v_y \\ &= -u_{\infty} [1 + R_c^2 / (x^2 + y^2)] y / (x^2 + y^2)^{-0.5} ; \end{aligned}$$

$$\begin{aligned} u_r &= x(x^2 + y^2)^{-0.5} v_x + y(x^2 + y^2)^{-0.5} v_y \\ &= u_{\infty} [1 - R_c^2 / (x^2 + y^2)] x / (x^2 + y^2)^{-0.5} ; \end{aligned}$$

$$-y u_x + x u_y = -u_{\infty} [1 + R_c^2 / (x^2 + y^2)] y ;$$

$$x u_x + y u_y = u_{\infty} [1 - R_c^2 / (x^2 + y^2)] x .$$

From the last two equations were calculated velocities,  $u_x$  and  $u_y$

$$u_x = u_{\infty} [1 - R_c^2 (x^2 - y^2) / (x^2 + y^2)^2] ; \quad (1-6)$$

$$u_y = -2u_{\infty} R_c^2 xy / (x^2 + y^2)^2 . \quad (1-7)$$

From relation  $y = r \sin \theta$  one can obtain stream function easily in dimensionless way from equation (1-3)

$$\psi = u_{\infty} y [1 - R_c^2 / (x^2 + y^2)] ; \quad (1-8)$$

equations (1-6), (1-7), (1-8) can be nondimensionalized by setting

$$x' = x/R_C ; y' = y/R_C ; \Delta x' = \Delta x/R_C ; \Delta y' = \Delta y/R_C ;$$

$$t' = tu_\infty/R_C ; u' = u_x/u_\infty ; u'_y = u_y/u_\infty ; \psi' = \psi/(u_\infty R_C) .$$

with these, equations (1-6), (1-7), (1-8) become

$$u'_x = 1 - (y'^2)/(x'^2 + y'^2)^2 , \quad (1-9)$$

$$u'_y = -2x'y'/(x'^2 + y'^2)^2 , \quad (1-10)$$

$$\psi' = y' [1 - 1/(x'^2 + y'^2)] . \quad (1-11)$$

For potential flow with electric force the particle trajectory can be deduced from the equation of particle motion (velocity components  $v_x, v_y$ ) in which the gravitational force will be neglected:

$$dv/dt = -(C_D R_e / 24K)(v-u) - C_e e_r , \quad (1-12)$$

$C_e = F_e R_C / (u_\infty^2 K^{0.5} r'^2)$ , where  $K = 2pr^2 u_\infty / 9\mu R_C$  is the Stokes number, and  $F_e = Q_A Q_B K^{0.5} / R_C L_m$  is a Coulomb force number, i.e.  $C_e e_r$  is the dimensionless Coulomb force between two point charges  $Q_A$  and  $Q_B$  separated by a distance  $r = r' R_C$ .

The transformation of Coulomb force number and electrostatic force term is as follows:

$$F_e = K_0 Q_A Q_B / r^2 ; m_p = 4\pi r_p^3 \rho_p / 3$$

hence

$$F_e / m_p = 3K_0 Q_A Q_B / (4\pi r_p^3 \rho_p^3) . \quad (1-13)$$

1 Coulomb =  $3 \times 10^9$  e.s.u., 1 newton =  $10^5$  dyne, therefore

$$K_0 = 1 \text{ dyne} \cdot \text{cm}^2 / (\text{e.s.u.})^2 ,$$

let  $Q'_A = Q_A / (L R_C)$ ,  $Q'_B = Q_B / r_p^2$ , the electrostatic force term becomes

$$(3Q_A'Q_B')/(4\pi r_p \rho_p r^2) \cdot (R_C^2 L/u_\infty^2) e_r =$$

$$[3Q_A'Q_B'/(4\pi)][2u_\infty/(9\mu\rho_p R_C)]^{0.5}/[\rho_p r_p^2 u_\infty/(9\mu R_C)]^{0.5} L/(u_\infty^2 r^2) e_r.$$

Let

$$F_E = [3Q_A'Q_B'/(4\pi)][2u_\infty/(9\mu\rho_p R_C)]^{0.5} =$$

$$= Q_A'Q_B'K^{0.5}/(LR_{cm_p}) \quad (1-14)$$

be the Coulomb force number. Then the corresponding electrostatic force term is

$$C_e e_r = [2\rho_p r_p^2 u_\infty/(9\mu R_C)]^{-0.5} \cdot F_E L/(u_\infty^2 r^2) e_r.$$

At this point Bergrun's scheme is modified to get the equation of trajectory of particles

$$v_x dv_x/dx = -(C_D R_e/24K)(v_x - u_x) - C_e \cos\theta, \quad (1-15)$$

$$v_y dv_y/dy = (C_D R_e/24K)(v_y - u_y) + C_e \sin\theta, \quad (1-16)$$

$$dx/dt = -v_x - C_e \cos\theta, \quad dy/dt = -v_y + C_e \sin\theta,$$

$$(R_c/N_{Re})^2 = (v_x - u_x)^2 + (v_y - u_y)^2. \quad (1-17)$$

The velocity and position of a particle at the end of any interval of time may be expressed by the following equations:

$$v_x(n+1) = v_x(n) - (C_D R_c/24K)(v_x(n) - u_x(n)) \Delta t - C_e \cos\theta \Delta t, \quad (1-18)$$

$$v_y(n+1) = v_y(n) - (C_D R_c/24K)(v_y(n) - u_y(n)) \Delta t + C_e \sin\theta \Delta t, \quad (1-19)$$

$$x(n+1) = v_x(n) t - 0.5(C_D R_c/24K)(v_x(n) - u_x(n)) t^2 - 0.5C_e \cos\theta \Delta t^2, \quad (1-20)$$

$$y(n+1) = v_y(n) t - 0.5(C_D R_c/24K)(v_y(n) - u_y(n)) t^2 + 0.5C_e \sin\theta \Delta t^2. \quad (1-21)$$

Assume the initial velocity of the particle to be the same as that of the air at a fairly large distance forward of the cylinder; then one can estimate the second velocity of the particle both in the X and Y directions. The relevant relation is given in Appendix B.

$$v_{x1} = 0.5 \{ (u_{x0} - \Delta xH) + [(u_{x0} - \Delta xH)^2 + 4(u_{x1} \Delta yH + \Delta xC_e \cos \theta)]^{0.5} \} \quad (1-22)$$

$$v_{y1} = 0.5 \{ (u_{y0} - \Delta yH) + [(u_{y0} - \Delta yH)^2 + 4(u_{y1} \Delta yH + \Delta yC_e \sin \theta)]^{0.5} \} \quad (1-23)$$

A listing of the computer program is attached.

APPENDIX  
LISTING OF PROGRAM

```

c THIS PROGRAM COMPUTES DROP TRAJECTORIES PAST A CYLINDER IN
c POTENTIAL FLOW WITH ELECTRIC CHARGE (IN CARTESIAN COORDINATE)
c RELAXATION TIME: TAU=(2*RP*RP*RHOP)/(9*MEUA)
c STREM(I)=UINF*ETA(I)*(1-RC*RC/(PSI(I)**2+ETA(I)**2))
c STROKE'S NO : ST=TAU*UINF/RC
c LENGTH UNIT : CM - BUT IN DIMENSIONLESS WAY
c CHARGE UNIT : ELECTROSTATIC UNIT
c
REAL MEU, MASSP
COMMON MEU, RHOA, RHOP, RC, RP, N, VX(400), VY(400), K, AR, QAA, QBB, RENOC
DIMENSION VPSI(400), VETA(400), PSI(400), ETA(400), RENOL(400),
5 COEF(400), ELEF(400), RSQ(400), DIST(400), COST(400),
5 SINT(400)
CALL INITT(960)
CALL TERM(3, 1024)
CALL CHRST(4)
CALL DWINDO(-6.0, 2.0, -2., 4.)
CALL TWINDO(100, 900, 100, 700)
CALL ANMODE
READ(5, *) RHOA, RHOP, MEU, N
READ(5, *) RENOC, DC, DP, AR, QAA, QBB
RP=0.5*DP
RC=0.5*DC
UINF=RENOC*MEU/(DC*RHOA)
WRITE(6, 4) DC, DP, UINF, RHOP, AR, RENOC
4 FORMAT(1X, '***DC=', E12.5, 1X, '***DP=', E12.5, 1X, '***UINF=', F10.4/1X, '***
SRHOP=', F5.2, 1X, '***RATIO AR =', E12.5, 1X, '***RENOC =', F10.3)
WRITE(6, 22) QAA, QBB
22 FORMAT(1X, 'QAA=', F6.2, 1X, 'QBB=', F6.2)
CALL CIRCLE
DO 55 K=1, 12
CALL ANMODE
READ(5, *) FS
WRITE(6, 80) FS
80 FORMAT(/, 1X, '***FS=', E12.6)
CALL DISP(UINF, PSI, ETA, FS, I)
CALL MOVABS(100, 300)
55 CONTINUE
CALL FINITT(0, -300)
STOP
END
-----
c ROUTINE FOR CALCULATING THE VELOCITY OF FREE STREAM
SUBROUTINE FREST(UINF, I, FS)
REAL MEU
COMMON MEU, RHOA, RHOP, RC, RP, N, VX(400), VY(400), K, AR, QAA, QBB, RENOC
N=-6.1
P1=1.
P2=-FS

```

```

YY=0.10286*K
CALL MOVEA(-6.0,YY)
DO 50 I=1,N
X=X+0.1
P3=X*X-1.
P4=-FS*X*X
CALL SOLVE(P1,P2,P3,P4,Y1,Y2,Y3)
CALL DRAWA(X,Y1)
A=X*X+Y1*Y1
D=X*X-Y1*Y1
B=A*A
VX(I)=1.-D/B
VY(I)=-2.*X*Y1/B
50 CONTINUE
CALL MOVEA(-6.0,YY)
RETURN
END

```

c.....

c.....

c.... ROUTINE FOR SOLVING CORRESPONDING Y COORD FOR EACH X COORD

```

SUBROUTINE SOLVE(P1,P2,P3,P4,Y1,Y2,Y3)
F(YY)=P1*YY**3+P2*YY*YY+P3*YY+P4
G(YY)=3.*P1*YY*YY+2.*P2*YY+P3
EPS=1.E-04
II=-2
JJ=0
YI=0.
15 Y=YI+5.
2 YI=Y-F(Y)/G(Y)
JJ=JJ+1
IF(JJ.EQ.100) GO TO 10
IF(ABS(F(YI))-EPS) 4,3,3
3 Y=YI
GO TO 2
4 II=II+1
IF(II) 7,6,9
7 Y1=YI
GO TO 5
8 Y2=YI
GO TO 5
9 Y3=YI
5 IF(II.NE.1) GO TO 15
GO TO 12
10 WRITE(6,11)
11 FORMAT(1X,'*** THE SOLUTION OF Y CAN NOT CONVERGE')
12 CONTINUE
RETURN
END

```

c.....

c.....

c.... ROUTINE FOR CALCULATING THE DISPLACEMENT OF PARTICLE

```

SUBROUTINE DISP(UINF,PSI,ETA,FS,I)
REAL MEU,MASSP

```

```

COMMON NEU, RHOA, RHOP, RC, RP, N, VX(400), VY(400), K, AR, QAA, QBB, RENOC
DIMENSION VPSI(400), VETA(400), PSI(400), ETA(400),
$      RENOL(400), COEF(400), ELEF(400), RSQ(400),
$      DIST(400), COST(400), SINT(400)
DELPS=0.1
PSI(1)=-6.0
ETA(1)=0.10286*K
PSI(2)=PSI(1)+DELPS
CALL FREST(UINF, I, FS)
CALL MOVEA(PSI(1), ETA(1))
VPSI(1)=VX(1)
VETA(1)=VY(1)
DELET=VY(1)/VX(1)*DELPS
ETA(2)=ETA(1)+DELET
PI=3.1415926
MASSP=4./3.*PI*RP**3*RHOP
WRITE(6,90)MASSP
90 FORMAT(1X, 'MASSP=', E12.6)
c.... CALCULATE THE REYNOLD NUMBER OF FREE STREAM
RENOP=RHOA*UINF*RP**2./NEU
WRITE(6,5)DELET
5 FORMAT(1X, 'DELET=', E12.6)
WRITE(6,8)RENOP
8 FORMAT(1X, 'RENOP=', F8.3)
c.... CALCULATE THE RELAXATION TIME
TAU=2.*RP*RP/RHOP/(9.*NEU)
ST=TAU*UINF/RC
WRITE(6,11)ST,TAU
11 FORMAT(1X, 'ST=', E12.6, 1X, 'TAU=', E12.6)
RENOL(1)=0.
COEF(1)=1.
RSQ(1)=PSI(1)**2+ETA(1)**2
DIST(1)=SQRT(RSQ(1))
C
C THE X AND Y COMPONENT RELATED TO THE ELECTRIC CHARGE
C
COST(1)=PSI(1)/DIST(1)
SINT(1)=ETA(1)/DIST(1)
C
c.... FIND THE LENGTH OF CYLINDER
CLENG=RC/AR
C
c.... FIND THE MASS OF CYLINDER
CMASS=3.1415926*RC*RC*CLENG
RMASS=MASSP/CMASS
WRITE(6,91)CLENG,CMASS,RMASS
91 FORMAT(1X, '#CLENG=', E12.5, 1X, 'CM', 1X, '#CMASS=', E12.5, 1X, 'GM'/1X,
$ '#RMASS=', E12.5)
IF (RMASS-0.001) 44,44,55
C
C ELECTRIC CHARGE DATA IN DIMENSIONLESS WAY
C
44 QA=RC*CLENG*QAA

```

```

QB=RP*RP*QBB
WRITE(6,111)QA,QB
111 FORMAT(1X,'QA=',E12.5,1X,'QB=',E12.5)
C
c... INITIAL VALUE OF COULOMB FORCE NUMBER AND ELECTRIC TERM
c
FE1=QA*QB*ST**0.5/(RC*MASSP*CLENG)
ELEF(1)=FE1*CLENG/(UINF**2*ST**0.5*RSQ(1))
WRITE(6,110)FE1,ELEF(1)
110 FORMAT(1X,'**FE1=',E12.5,1X,'**ELEF(1)=' ,F12.5)
C
c... CALCULATE THE SECOND VALUE OF VELOCITY OF PARTICLE
A=-VX(1)+1./ST*DELPS
B=A*A+4.*(VX(2)*DELPS/ST-DELPS*ELEF(1))*COST(1)
C=SQRT(B)
VPSI(2)=(-A+C)/2.
D=1./ST*DELET-VY(1)
E=D*D+4.*(VY(2)*DELET/ST+DELET*ELEF(1))*SINT(1)
F=SQRT(E)
VETA(2)=(-D+F)/2.
DELT=0.1
AA=PSI(1)
BB=ETA(1)
CALL MOVEA(AA,BB)
DO 50 I=1,N
RSQ(I+1)=(PSI(I+1)**2+ETA(I+1)**2)
DIST(I+1)=SQRT(RSQ(I+1))
COST(I+1)=PSI(I+1)/DIST(I+1)
SINT(I+1)=ETA(I+1)/DIST(I+1)
c... CALCULATE THE LOCAL REYNOLD NO FROM THE RELATION THAT REYNOLD NO
C OF FLOW FIELD TIMES LOCAL VELOCITY
VXDIF=(VPSI(I+1)-VX(I+1))**2
VYDIF=(VETA(I+1)-VY(I+1))**2
RENOL(I+1)=RENOF*(VXDIF+VYDIF)**0.5
COEF(I+1)=1.+0.197*RENOL(I+1)**0.63+0.00026*RENOL(I+1)**1.38
H=COEF(I+1)/ST
HH=SQRT(ST/COEF(I+1))
C
c... COULOMB FORCE NUMBER
c
FE=QA*QB*HH/(RC*MASSP*CLENG)
C
c... ELECTRIC FORCE TERM
c
ELEF(I+1)=FE*CLENG/(UINF**2*HH*RSQ(I+1))
C... CALCULATE THE DISPLACEMENT OF THE PARTICLE
PSI(I+2)=VPSI(I+1)*DELT-0.5*H*(VPSI(I+1)-VX(I+1))*DELT**2
S +PSI(I+1)-0.5*ELEF(I+1)*COST(I+1)*DELT**2
ETA(I+2)=VETA(I+1)*DELT-0.5*H*(VETA(I+1)-VY(I+1))*DELT**2
S +ETA(I+1)+0.5*ELEF(I+1)*SINT(I+1)*DELT**2
c... CALCULATE THE VELOCITY OF PARTICLE
VPSI(I+2)=VPSI(I+1)-H*(VPSI(I+1)-VX(I+1))*DELT
S -ELEF(I+1)*COST(I+1)*DELT

```

```

VETA(I+2)=VETA(I+1)-H*(VETA(I+1)-VY(I+1))*DELT
S      +ELEF(I+1)*SINT(I+1)*DELT
WRITE(6,24)I,VPSI(I),I,VETA(I)
24 FORMAT(/1X,'VPSI(',I3,')=' ,E12.6,3X,'VETA(',I3,')=' ,E12.6)
SQ=SQRT(PXI(I)**2+ETA(I)**2)
EPS=ABS(SQ)-1.
RATIO=RP/RC
IF(EPS.LE.RATIO) GO TO 20
CALL DASHA(PXI(I),ETA(I),3)
WRITE(6,22)I,PXI(I),I,ETA(I)
22 FORMAT(/1X,'PXI(',I3,')=' ,E12.6,3X,'ETA(',I3,')=' ,E12.6)
GO TO 50
20 CALL ANNODE
WRITE(6,21)I,PXI(I),I,ETA(I)
21 FORMAT(/1X,'THE CRITICAL PT: ' /1X,'PXI(',I3,')=' ,E12.6,3X,
S      'ETA(',I3,')=' ,E12.6)
GO TO 55
50 CONTINUE
55 RETURN
END

```

c.....

c.....

c.... DRAW A CIRCLE DIVIDED BY 60 POINTS WITH CENTER O(0.,0.), DIAMETER

c.... CD= 1. IN DIMENSIONLESS WAY

SUBROUTINE CIRCLE

CALL POINTA(0.0,0.0)

A=2.\*3.1415926/60.

I1=100\*COS(A)

I2=100\*SIN(A)

CALL MOVREL(I1,I2)

DO 5 I=2,61

B=A\*I

IX=100\*COS(B)

IY=100\*SIN(B)

IA=IX-I1

IB=IY-I2

I1=IX

I2=IY

CALL DRWREL(IA,IB)

5 CONTINUE

RETURN

END

APPENDIX - B

VISCOUS FLOW PAST AN INFINITE CYLINDER

Schlamp (1977) assumed a steady-state viscous flow normal to an infinitely long cylinder with the free stream velocity  $U_\infty$  of the fluid. The Stokes-Navier and continuity equations are then

$$\vec{u} \cdot \nabla \vec{u} = -\nabla P / \rho + \nu \nabla^2 \vec{u} , \quad (2-1)$$

$$\nabla \cdot \vec{u} = 0 . \quad (2-2)$$

Considering well-known vector relations one can deduce from Eqs. (2-1) and (2-2)

$$\nabla \times (\nu \nabla^2 \vec{u}) = -\nabla \times \{ \vec{u} \times (\nabla \times \vec{u}) \} . \quad (2-3)$$

Velocities and other parameters have in two dimensional, polar coordinates the form

$$\vec{u} = e_z \times \nabla \psi ; u_r = -1/r (\partial \psi / \partial \theta) ; \zeta = \nabla \times \vec{u} = e_z \nabla^2 \psi ; u_\theta = \partial \psi / \partial r , \quad (2-4)$$

where  $e_z$  is unit vector in z direction,  $\psi$  the stream function and  $\zeta$  the vorticity. We now nondimensionalize the relationships in the usual way

$$r' = r/R_c, \vec{u}' = \vec{u}/u_\infty, \psi' = \psi/u_\infty R_c, N_{Re} = 2r_p u_\infty / \nu, \zeta' = \zeta R_c / u_\infty . \quad (2-5)$$

From Eq. (2-3) one then finds, after dropping the primes for convenience,

$$\nabla^2 (\nabla \times \vec{u}) = 0.5 N_{Re} \nabla \times \{ \vec{u} \times (\nabla \times \vec{u}) \} , \quad (2-6)$$

and with equation (2-4)

$$\nabla^2 (\nabla \times \vec{u}) = 0.5 N_{Re} \nabla \times \{ (e_z \times \nabla \psi) \times (\nabla \times (e_z \times \nabla \psi)) \} . \quad (2-7)$$

Using standard vector operations, one may write the nondimensional Navier Stokes equations as

$$\nabla^4 \psi = 0.5 N_{Re} \{ (\partial \psi / \partial r) (\partial (\nabla^2 \psi) / \partial \theta) - (\partial \psi / \partial \theta) (\partial (\nabla^2 \psi) / \partial r) \} / r . \quad (2-8)$$

More conveniently, equation (2-8) may be split in two second-order differential equations by introducing the vorticity  $\zeta$ . This gives

$$\nabla^2 \zeta = 0.5 N_{Re} \{ (\partial \psi / \partial r) (\partial \zeta / \partial \theta) - (\partial \psi / \partial \theta) (\partial \zeta / \partial r) \} ,$$

$$\text{with } \zeta = \nabla^2 \psi, \text{ where } \nabla^2 = \partial^2 / \partial r^2 + 1/r^2 (\partial^2 / \partial \theta^2) + \frac{1}{r} (\partial / \partial r) . \quad (2-9)$$

Near the cylinder surface at small  $Re$ , a small radial step size is needed where the stream function and the vorticity vary most rapidly. The customary procedure with  $r = e^z$  was used for a constant step size  $\Delta z$ . Equation (2-9) then becomes

$$\nabla^2 \zeta = 0.5 N_{Re} \{ (\partial \psi / \partial z) (\partial \zeta / \partial \theta) - (\partial \psi / \partial \theta) (\partial \zeta / \partial z) \} , \quad (?-10)$$

$$\text{with } \zeta = e^{2z} \nabla^2 \psi, \text{ where } \nabla^2 = \partial^2 / \partial z^2 + \partial^2 / \partial \theta^2 .$$

Boundary conditions are along the axis of symmetry:  $\theta = 0, \pi, \psi = 0, \zeta = 0$ . On cylinder surface:  $z = 0, \psi = 0, \zeta = \nabla^2 \psi, \partial \psi / \partial z = 0$ . On cylindrical boundary concentric with but remote from cylinder surface:  $z = z_\infty, \psi = e^{2z_\infty} \sin \theta, \zeta = 0$ .

The flow pattern about an infinite length cylinder is displayed in Figure A.2-I, which shows that considerable fore-aft asymmetry is already apparent for  $N_{Re} = 1$ . At  $N_{Re} = 20$ , a standing eddy of sizeable dimensions has developed at the reverse side of the cylinder (Schlamp, 1977).

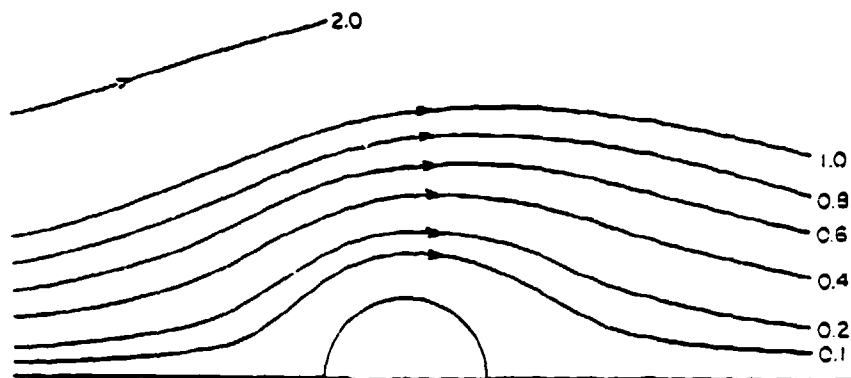


Fig. B-1a.  $N_{Re} = 1.0$ .

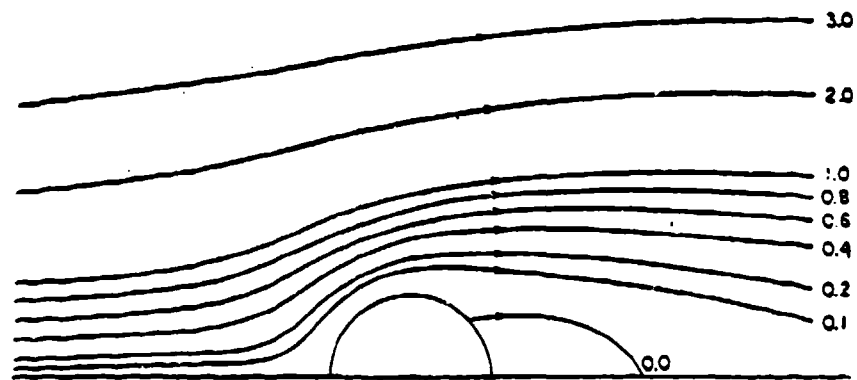


Fig. B-Ib.  $N_{Re} = 2.0$ .

All calculations used for the flow field about an infinite cylinder were based on the Ph.D. thesis by Dr. R.J. Schlamp (UCLA, 1977) and on his conversion of Navier-Stokes equations in finite difference equation. The applied technique can be summarized as follows: The first and second derivations of basic functions are

$$\frac{\partial \psi}{\partial z} \Big|_{(I,J)} = \{\psi(I,J+1) - \psi(I,J-1)\} / 2A \quad (2-11)$$

$$\nabla^2 \zeta / \partial r^2 \Big|_{(I,J)} = \{\zeta(I+1,J) - 2\zeta(I,J) + \zeta(I-1,J)\} / B^2 \quad (2-12)$$

One can rewrite the equation (2-9) using finite difference formulas to obtain

$$\begin{aligned} & \{(\psi(I,J+1) - \psi(I,J-1)) / 2A\} \{(\zeta(I+1,J) - \zeta(I-1,J)) / 2B\} - \{(\psi(I+1,J) \\ & - \psi(I-1,J)) / 2B\} \{[\zeta(I,J+1) - \zeta(I,J-1)] / 2A\} = \\ & 2\{[\{\zeta(I,J+1) - 2\zeta(I,J) + \zeta(I,J-1)\} / A^2] + [\{\zeta(I+1,J) - 2\zeta(I,J) \\ & + \zeta(I-1,J)\} / B^2]\} / N_{Re} \quad (2-13) \end{aligned}$$

This equation can then be solved for  $\zeta(I, J)$  to obtain

$$\begin{aligned} \zeta^{(n+1)}(I, J) = & [(0.5A^2B^2/(A^2+B^2))\{\zeta^{(n)}(I, J+1)[1/A^2 + N_{Re}[\psi^{(n)}(I+1, J) \\ & - \psi^{(n)}(I-1, J)]/8AB\} + \zeta^{(n)}(I, J-1)[1/A^2 - N_{Re}[\psi^{(n)}(I+1, J) \\ & - \psi^{(n)}(I-1, J)]/8AB\} + \zeta^{(n)}(I+1, J)[1/B^2 - N_{Re}\{(\psi^{(n)}(I, J+1) - \psi^{(n)} \\ & (I, J-1))/8AB\} + \zeta^{(n)}(I, J-1)[1/B^2 - N_{Re}\{(\psi^{(n)}(I, J+1) - \psi^{(n)} \\ & (I, J-1))/8AB\}] , \end{aligned} \quad (2-14)$$

where  $n$  and  $n+1$  introduce the concept of an iteration step. Similarly, if the vorticity equation (2-9) is expressed using finite difference formulas and solved for  $\psi(I, J)$ , one obtains for the outlined boundary conditions

$$\begin{aligned} \psi^{(n+1)}(I, J) = & [0.5A^2B^2/(A^2+B^2)]\{[\psi^{(n)}(I, J+1) - \psi(I, J-1)] \\ & /A^2\} + \{[\psi^{(n)}(I+1, J) + \psi^{(n)}(I-1, J)]/B^2\} - \exp[2z(J)]\zeta^{(n)}(I, J) \} . \end{aligned} \quad (2-15)$$

Using equation (2-10) one finds for the side boundaries

$$I=1, N+1 ; \psi(1, J)=0, \zeta(1, J)=0 ,$$

and for the cylinder surface

$$J=1 ; \psi(I, 1)=0, \zeta^{(n+1)}(I, 1)=0.5A^2\{8\psi^{(n)}(I, 2) - \psi^{(n)}(I, 3)\} .$$

For the cylindrical boundary remote from the collector

$$J=N; \psi(I, N)=\exp z(N)\sin(I) , \zeta(I, N)=0 .$$

APPENDIX C

TWO HYDRODYNAMICALLY INTERACTING CYLINDERS

The flowfield between two identical interacting cylinders can be described following the scheme in Fig. C-I. Elementary trigonometric operations lead to the deduction of the velocity components in the radial and tangential direction around the reference cylinder.

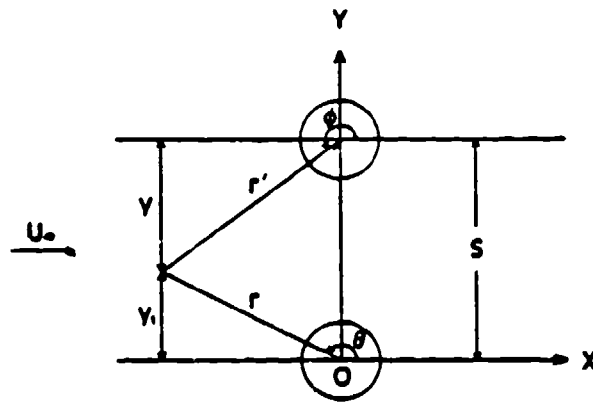


Fig. C-I

$$U_r = U_\infty \left(1 - \frac{R^2}{r^2}\right) \cos\theta - U_\infty \frac{R^2}{r'^2} \cos\psi \quad (3-1)$$

$$U_\theta = -U_\infty \left(1 + \frac{R^2}{r^2}\right) \sin\theta - U_\infty \frac{R^2}{r'^2} \sin\psi \quad (3-2)$$

where  $r'^2 = r^2 + s^2 - 2rs \sin\theta$ . From (3-1) one obtains

$$\begin{aligned} U_r &= U_\infty \left(1 - \frac{R^2}{x^2 + y^2}\right) \frac{x}{\sqrt{x^2 + y^2}} - U_\infty \frac{R^2}{[x^2 + (s-y)^2]} \frac{x}{\sqrt{x^2 + (s-y)^2}} = \\ &= \frac{x}{\sqrt{x^2 + y^2}} U_x + \frac{y}{\sqrt{x^2 + y^2}} U_y \end{aligned} \quad (3-3)$$

and in a similar way from (3-2) results

$$U_\theta = -U_\infty \left(1 + \frac{R^2}{x^2 + y^2}\right) \frac{y}{\sqrt{x^2 + y^2}} - U_\infty \frac{R^2}{[x^2 + (s-y)^2]} \frac{(y-s)}{\sqrt{x^2 + (s-y)^2}} =$$

$$= \frac{-y}{\sqrt{x^2+y^2}} U_x + \frac{x}{\sqrt{x^2+y^2}} U_y \quad (3-4)$$

For the numerical calculation of particle deposition on cylinders the flowfield coordinates were converted into a nondimensional cartesian system with components

$$U'_x = 1 + \frac{-2x'y'}{(x'^2+y'^2)^2} + \frac{(y'^2 - x'^2 - \frac{y'S}{R})}{x'^2+y'^2 \cdot x'^2 + (\frac{S}{R} - y')^2 \cdot x'^2 + (\frac{S}{R} - y')^2} \quad (3-5)$$

$$U'_y = \frac{-2x'y'}{(x'^2+y'^2)^2} + \frac{(\frac{x'S}{R})}{\sqrt{x'^2+y'^2} \sqrt{x'^2 + (\frac{S}{R} - y')^2} [x'^2 + (\frac{S}{R} - y')^2]} \quad (3-6)$$

The dimensionless parameters are

$$U'_x = \frac{U_x}{U} ; U'_y = \frac{U_y}{U} ; x' = \frac{x}{R} ; y' = \frac{y}{R} .$$

The calculation of particle trajectory from the flowfield and known physical properties of the particle is identical to the procedure described in Appendix A.

APPENDIX D

BROWN'S MODEL FOR MANY-FIBER VISCOUS FLOW

The many-fiber viscous flow model (Brown, 1994) is based on the Helmholtz theorem of the viscous flow pattern--which adjusts to the lowest rate of dissipation of energy--and on the formulation of a stream function for a filter fiber array with the aid of the stream function with spacial periodicity (Kirsch and Fuchs, 1967)

$$\psi = \bar{U}_x y + \bar{U}_x l \sum_{n=1}^{\infty} \sum_{k=0}^{\infty} a_{nk} \sin \frac{n\pi y}{l} \cos \frac{k\pi x}{e} \quad (4-1)$$

The stream function was deduced for channel and staggered model which are depicted in Fig. D-I.



Fig. D-I

The formula for energy dissipation in viscous flow is

$$\theta = \eta \iiint \left\{ 2 \left( \frac{\partial u_x}{\partial x} \right)^2 + 2 \left( \frac{\partial u_y}{\partial y} \right)^2 + 2 \left( \frac{\partial u_z}{\partial z} \right)^2 + \left( \frac{\partial u_y}{\partial z} + \frac{\partial u_z}{\partial y} \right)^2 + \left( \frac{\partial u_z}{\partial x} + \frac{\partial u_x}{\partial z} \right)^2 + \left( \frac{\partial u_x}{\partial y} + \frac{\partial u_y}{\partial x} \right)^2 \right\} dx dy dz \quad (4-2)$$

For the two-dimensional case with flow through an array of fibers extended in the z-direction Eq. (4-2) can be rewritten in terms of stream function

$$\theta = \iiint \left\{ \left( \frac{\partial^2 \psi}{\partial y^2} + \frac{\partial^2 \psi}{\partial x^2} \right)^2 + 4 \left( \frac{\partial^2 \psi}{\partial x \partial y} \right)^2 \right\} dx dy \quad (4-3)$$

After calculating the terms of  $\frac{\partial^2 \psi}{\partial y^2}$ ,  $\frac{\partial^2 \psi}{\partial x^2}$  and  $\frac{\partial^2 \psi}{\partial x \partial y}$  from Eq. (4-1) and substituting them into Eq. (4-3) the rate of energy dissipation will be

$$\theta = \eta U_{\infty}^2 \pi^4 e \ell^3 \left\{ \sum_{n=1}^{\infty} 2a_{n0}^2 \frac{n^4}{4} + \sum_{n=1}^{\infty} \sum_{k=1}^{\infty} a_{nk}^2 \left( \frac{n^2}{\ell^2} + \frac{k^2}{e^2} \right) \right\} \quad (4-4)$$

The values of  $a_{nk}$  that give the minimum energy dissipation and satisfy the boundary condition (stream function vanish at points close together), are

$$y_{i+\ell} \sum_{n=1}^{\infty} \sum_{k=0}^{\infty} a_{nk} \frac{n\pi y_i}{\ell} \cos \frac{k\pi x_i}{e} = 0 \Rightarrow a_{nk} = \frac{-y_i}{\ell \sin \frac{n\pi y_i}{\ell} \cos \frac{k\pi x_i}{e}} \quad (4-5)$$

and the condition of minimum energy dissipation yield

$$\frac{\partial}{\partial a_{nk}} \left\{ \sum_{n=1}^{\infty} 2a_{n0}^2 \frac{n^4}{4} + \sum_{n=1}^{\infty} \sum_{k=1}^{\infty} a_{nk}^2 \left( \frac{n^2}{\ell^2} + \frac{k^2}{e^2} \right) + \right. \quad (4-6)$$

$$\left. + \sum_{i=1}^M \gamma_i [y_{i+\ell} \sum_{n=1}^{\infty} \sum_{k=0}^{\infty} a_{nk} \sin \frac{n\pi y_i}{\ell} \cos \frac{k\pi x_i}{e}] \right\} = 0$$

In Eq. (4-6)  $M$  are the points close to the cylinder surface  $x_i, y_i$ , where the stream function vanishes and  $\gamma_i$  are Lagrangean undetermined multipliers. Differentiation with respect to each  $a_{nk}$  gives an equation that involves no other  $a_{nk}$ . The resulting equation for  $a_{nk}$  is

$$a_{nk} f(n,k) + \sum_{i=1}^M \gamma_i \ell \sin \frac{n\pi y_i}{\ell} \cos \frac{k\pi x_i}{e} = 0 \quad (4-7)$$

with

$$f(n,0) = 4 \frac{n^4}{\ell^4}; \quad f(n,k) = 2 \left( \frac{n^2}{\ell^2} + \frac{k^2}{e^2} \right)^2 \text{ for } k \neq 0.$$

Substituting  $a_{nk}$  from (4-5) into (4-7) yields

$$\sum_{i=1}^M \gamma_i u_{ij} = \gamma_j, \text{ for } 1 \leq j \leq M \quad (4-8)$$

with

$$u_{ij} = \sum_{n=1}^{\infty} \sum_{k=0}^{\infty} \frac{\ell^2}{f(n,k)} \sin \frac{n\pi y_i}{\ell} \sin \frac{n\pi y_j}{\ell} \cos \frac{k\pi x_i}{e} \cos \frac{k\pi x_j}{e} \quad (4-9)$$

APPENDIX D

Equations (4-8) are solved by computer and the results (  $a_{nk}$  ) substituted into Eq. (4-7) for determining  $a_{nk}$ . Once  $a_{nk}$  is known, the stream function can be calculated from Eq. (4-1).

An example of streamline pattern around a parallel array of fibers for  $R = 2$ ,  $l = 10$ ,  $e = 10$  is presented in Fig. D-II

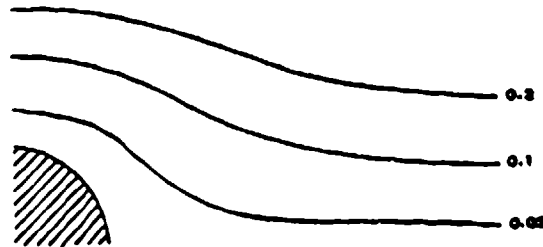


Fig. D-II (Brown, 1984)

and for staggered model in Fig. D-III (for  $R = 3$ ,  $l = 10$ ,  $e = 4$ ):

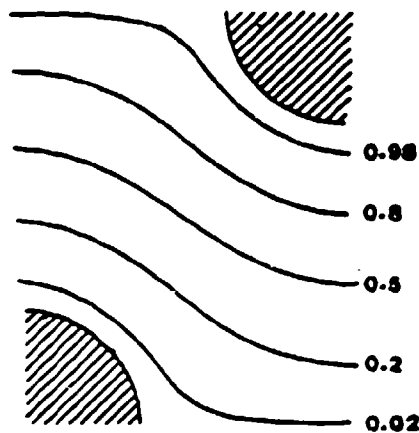


Fig. D-III (Brown, 1984)

For staggered model a stream function

$$\psi = \bar{u}_x y + \bar{u}_x \ell \sum_{\text{odd } n=1}^{\infty} \sum_{k=0}^{\infty} a_{nk} \sin \frac{n\pi y}{\ell} \cos \frac{(2k+1)\pi x}{2e} +$$

$$+ \bar{u}_x \ell \sum_{\text{even } n=2}^{\infty} \sum_{k=0}^{\infty} a_{nk} \sin \frac{n\pi y}{\ell} \cos \frac{k\pi x}{e}$$

is used in the same way as in the previous model, except the

odd-n terms where the following substitution is made

$$\cos \frac{k\pi x}{e} + \cos \frac{(2k+1)\pi x}{2e}$$

$$\left(\frac{n^2}{2} + \frac{k^2}{e^2}\right)^2 \left[\frac{n^2}{2} + \frac{(2k+1)^2}{(2e)^2}\right]^2 .$$

When the flowfield in the many fiber array is known then the particle deposition on each fiber and each row (plane) of cylinders perpendicular to the airflow direction can be calculated according to the relationships outlined in Appendix A (marked in Fig. D-III). The main problem is still the realistic description of the changing flowfields inside the many-fiber scavenger--which is related to the pressure drop across the filter (Brown, 1984)--and the calculation of particle trajectories in the many layer array. The model seems to be more suitable for thin scavengers with several planes of fibers behind each other.

## APPENDIX - E

### PHYSICAL MODEL FOR THE FALLING SCAVENGER ZONE

The main assumptions taken as basis for the numerical model describing the evolution of a falling scavenger zone are as follows:

Scavengers will be dispersed homogeneously in a zone located at a specific level at time  $t = 0$  (e.g., 100 m or 5000 m). They start to settle, disperse, collect aerosol, and entrain the environmental air. Scavengers are supposed to assume within one second their constant settling (terminal) velocity, which has been justified by our previous systematic experiments.

The equations of air motion and scavenger concentration are similar to those suggested by Clark and List (1971). We also used the mixing ratio,  $q$  (ratio of the scavenger mass in kg to 1 kg of air) as a measure of scavenger concentration. In our equations the isotropic turbulence exchange coefficient,  $K_t$ , represents the interaction of the induced air motion and the turbulent atmosphere. The basic equations of the two dimensional model (Podzimek and Smith, 1986) are:

$$\frac{\partial u}{\partial t} + w \frac{\partial w}{\partial x} + w \frac{\partial u}{\partial z} = - \frac{\partial}{\partial x} \left( \frac{p}{\rho} \right) + K_t \nabla^2 u, \quad (5-1)$$

$$\frac{\partial w}{\partial t} + u \frac{\partial w}{\partial x} + w \frac{\partial w}{\partial z} = - \frac{\partial}{\partial z} \left( \frac{p}{\rho} \right) + K_t \nabla^2 w - gp, \quad (5-2)$$

$$\frac{\partial u}{\partial x} + \frac{\partial w}{\partial z} = 0 \quad (5-3)$$

for air velocity components,

$$\frac{\partial q}{\partial t} + \frac{\partial (qu)}{\partial x} + \frac{\partial}{\partial z} [q(w - v_s)] = 0 \quad (5-4)$$

for the scavenger mixing ratio, and

$$\frac{\partial}{\partial t} \iint \left[ \frac{1}{2} (u^2 + w^2) + gqz \right] dx dz = - \iint gq v_s dx dz -$$

$$- K_t \iint \left[ \left( \frac{\partial u}{\partial x} \right)^2 + \left( \frac{\partial u}{\partial z} \right)^2 + \left( \frac{\partial w}{\partial x} \right)^2 + \left( \frac{\partial w}{\partial z} \right)^2 \right] dx dz$$

(5-5)

for equilibrium of energy. The last equation can be rewritten in

terms of air kinetic energy,  $K = \iint 1/2(u^2 + w^2) dx dz$ , of potential energy,  $gQ = g \iint q dx dz$ ,  $gQ^2 = g \iint q z dx dz$  and energy dissipation [the last term in Eq. (5-5)]. Equations (5-4) and (5-5) were also used for calculation of the convective velocity of the center of scavenger mass zone,  $V_z = (\partial z / \partial t + V_S)$ , assuming that no scavenger has reached the ground ( $Q = \text{const.}$ ).

Velocity components,  $u$ ,  $w$  were calculated from the stream function,  $\psi$ ,

$$u = \frac{\partial \psi}{\partial z}; \quad w = - \frac{\partial \psi}{\partial x} \quad (5-6)$$

and are related to the vorticity function,  $\xi$ ,

$$\xi = \frac{\partial u}{\partial z} - \frac{\partial w}{\partial x} \quad (5-7)$$

by the Poisson equation,

$$\nabla^2 \psi = \xi \quad (5-8)$$

Further, the vorticity transport equation,

$$\frac{\partial \xi}{\partial x} = -u \frac{\partial \xi}{\partial x} - w \frac{\partial \xi}{\partial z} + K_t \left[ \frac{\partial^2 \xi}{\partial x^2} + \frac{\partial^2 \xi}{\partial z^2} \right] + g \frac{\partial q}{\partial x} \quad (5-9)$$

was derived by using Eqs. (5-6) and (5-7) to simplify Eqs. (5-1) and (5-2).

The initial and boundary conditions are apparent in Fig. E-1 and were adapted to the goals of specific numerical calculations. For each study the size of the velocity fields to be studied was selected to be  $(L, H)$  with a mesh spacing  $\Delta x = \Delta z \equiv \Delta$ , and the initial release height of the scavenger zone to be  $H_p$  (the bottom of the scavenger zone). Air and scavengers are initially at rest. Then the following boundary conditions were selected on each wall of the field (denoted by numbers in Fig. E-1:

$$\begin{aligned} \text{Wall 1, (symmetry boundary): } & u = 0; \quad \frac{\partial w}{\partial x} = 0, \quad \psi = 0; \quad \xi = 0. \\ \text{Wall 2, (slip wall): } & u = 0; \quad \frac{\partial u}{\partial z} = 0; \quad \psi = 0; \quad \xi_{i,j} = \xi_{i,j+1}. \\ \text{Wall 3, (still air boundary): } & u = 0; \quad w = 0; \quad \psi = 0, \quad \xi = 0. \\ \text{Wall 4, (still air boundary): } & w = 0; \quad u = 0, \quad \psi = 0; \quad \xi = 0. \end{aligned} \quad (5-10)$$

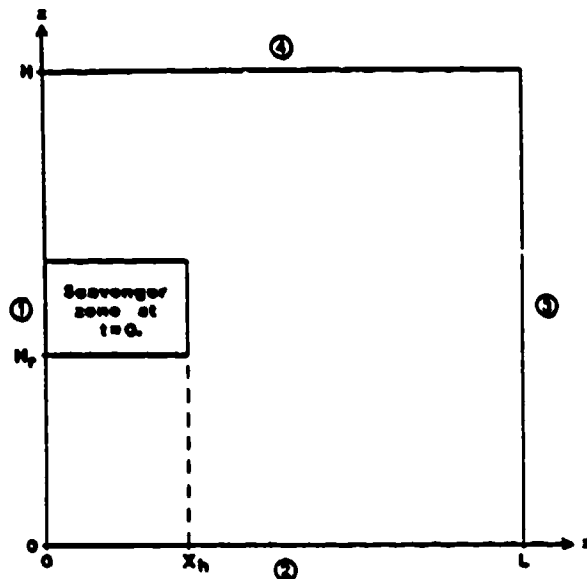


Fig. E-I

The following field dimensions (Fig. E-I) and parameters were selected for special investigations in the homogeneous calm atmosphere:

a) The impact of scavenger mixing ratio,  $q$ , on the induced downdraft velocity,  $w$ , and maximum width of the falling scavenger zone,  $b_{\max}$ :

$$q = 0.01 \text{ g sc./g air and } 0.04 \text{ g sc./g air;}$$

$$H = 10 \text{ km; } \quad V_S = 1.50 \text{ m/s;}$$

$$L = 10 \text{ km; } \quad K_t = 1000 \text{ m}^2/\text{s;}$$

$$H_R = 2 \text{ km;}$$

$$\text{Zone dimension: } 1 \text{ km} \times 1 \text{ km; mesh: } 20 \times 20.$$

b) The effect of changing the turbulent exchange coefficient,  $K_t$ , on the downdraft velocity,  $w$ , and dispersion of the scavenger zone:

$$q = 0.01 \text{ g sc./g air;}$$

$$H = 10 \text{ km; } \quad V_S = 6.0 \text{ m/s;}$$

$$L = 10 \text{ km; } \quad K_t = 1; 10; 100; 250; 500; 1000; 2500 \text{ m}^2/\text{s.}$$

$$H_R = 5 \text{ km;}$$

$$\text{Zone dimension: } 2 \text{ km} \times 2 \text{ km; mesh: } 20 \times 20.$$

c) The influence of the initial shape of the falling scavenger zone on the induced velocities,  $u$ ,  $w$ , and the dispersion of the scavengers:

$q = 0.01$  g sc./g air;  
 $H = 3$  km;  $V_S = 1.73; 1.50; 1.21$  m/s;  
 $L = 3$  km;  $K_t = 1000$  m<sup>2</sup>/s;  
 $H_R = 1$  km; mesh: 30 x 30.  
 Zone dimensions: 400 m x 400 m, 320 m x 500 m,  
 500 m x 320 m, 800 m x 200 m.

d) The effect of the low release height,  $H_R$ , and of the turbulent exchange coefficient,  $K_t$ , on the evolution of the downdraft,  $w$ :

$q = 0.01$  g sc./g air;  
 $H = 300$  m;  $V_S = 1.73$  m/s;  
 $L = 600$  m;  $K_t = 10$  and  $1000$  m<sup>3</sup>/s.  
 $H_R = 100$  m;  
 Zone dimension: 100 m x 100 m; mesh 12 x 24.

#### NUMERICAL MODEL CRITERIA

Numerical solutions of the above mentioned equations are based on the criteria as follows:

Stability equation for determining  $\Delta t_{max}$  (Pouache, 1932)

$$\Delta t \leq \frac{\Delta^2}{\alpha}, \text{ where } \alpha = 2216 \text{ m}^2/\text{s}.$$

Finite difference equation for the vorticity transport Eq. (5-9) is using forward time, central spacing differencing in fully explicit form

$$\frac{\xi_{i,j}^k - \xi_{i,j}^{k-1}}{\Delta t} = - \frac{u_{i,j}}{2\Delta} (\xi_{i+1,j}^k - \xi_{i-1,j}^k) - \frac{w_{i,j}}{2\Delta} (\xi_{i,j-1}^k - \xi_{i,j+1}^k) +$$

$$+ \frac{K_t}{\Delta^2} (\xi_{i+1,j} + \xi_{i-1,j} + \xi_{i,j-1} + \xi_{i,j+1} - 4\xi_{i,j}) + \frac{g}{2\Delta} (q_{i+1,j} - q_{i-1,j}) \quad (5-11)$$

The calculation of stream function,  $\psi$ , is based on the successive over-relaxation equation (Frankel, 1950; Young, 1954)

$$\psi_{i,j}^{k+1} = \psi_{i,j}^k + \frac{\omega_0}{4} (\psi_{i+1,j}^k + \psi_{i,j-1}^k - 4\psi_{i,j}^k - \Delta^2 \psi_{i,j}^k) \quad (5-12)$$

with an optimal over-relaxation factor approximated (Frankel, 1950) by

$$\omega_0 = 2 \left[ \frac{1 - \sqrt{1 - \xi}}{\xi} \right]; \quad \xi = \left[ \frac{\cos(\frac{\pi}{I-1}) + \cos(\frac{\pi}{J-1})}{2} \right]^2$$

I, J are numbers of nodes in x- and z-direction.

Scavenger distribution and deformation of the scavenger zone with the time was calculated under the assumption that regions of scavengers were represented by a tracer particles. These were expressed by the mixing ratio,  $q$  (calculated for the air mass in a specific cell), divided by the initial number of tracers in the cell. At the beginning of each time step, all tracers within the control zone of each node are summed up to calculate the new mixing ratio for each node.

Extending the above mentioned procedure into the evolution of scavenging cloud at horizontal wind velocity the following boundary conditions and scheme (in Fig. E-II) were accepted:

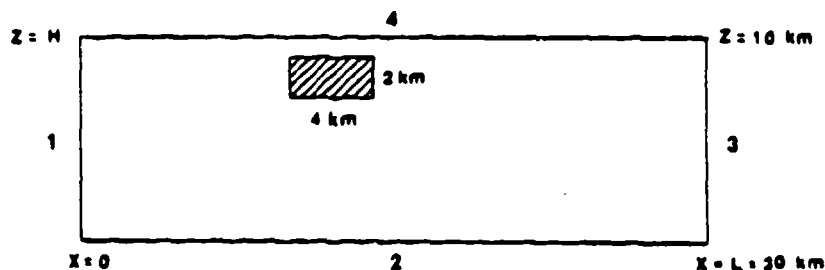


Fig. E-II

At the boundary 1

$$u = U_0 ; \xi = 0 ; \frac{\partial \psi}{\partial x} = 0 ,$$

at the boundary 2

$$w = 0 ; \xi_w = \xi_{w+1} \text{ (slip at the wall) ; } \psi = 0 ,$$

at the boundary 3

$$\xi = 0 ; \frac{\partial \psi}{\partial x} = 0 \text{ and}$$

at the boundary 4

$$w = 0 ; \xi = 0 ; \psi = U_0 H \text{ (from } u = \frac{\partial \psi}{\partial z} \text{) .}$$

PROGRAM ZONE;

(

This program was developed for the Graduate Center for Cloud Physics  
Research at the University of Missouri-Rolla under the direction of  
Dr. Josef Podzimek.

Scavenger Particle Zone release in a Horizontal Wind  
by Thomas E. Smith Jr. 1985 - 1986

This program is a 2-D finite difference model

)

(\$R+)

(\$I GRAPH.P :

(\$I SAVE.EXT)

TYPE

MIX P = ^MIX DAT ;

NODE P = ^NODE DAT ;

VEL P = ^VEL DAT ;

PART P = ^PART DAT ;

MIX DAT = ARRAY[-1..60] OF ARRAY[-1..20] OF REAL ;

NODE DAT = ARRAY[-1..60] OF ARRAY[-1..20] OF ARRAY[1..2] OF REAL ;

VEL DAT = ARRAY[-2..120] OF ARRAY[-2..40] OF REAL ;

PART DAT = ARRAY[1..800] OF REAL ;

CENTROID = ARRAY[0..50] OF REAL ;

VAR

OUT : TEXT ;

MIX, VIS : MIX P ; ( MIX = mixing ratio array, VIS = viscosity array )

VORT, SAI : NODE P ; ( VORT = vorticity array, SAI = stream function array )

U, W : VEL P ; ( U = X-dir. velocity array, W = Z-dir. velocity array )

XPOS, ZPOS : PART P ; ( XPOS = X-coord. array of tracer particles.

ZPOS = Z-coord. array of tracer particles )

XMEAN, ZMEAN : CENTROID ; ( XMEAN, ZMEAN = coordinates of centroid of zone )

NEWM, OLD, NEWB, I, J, K, T : INTEGER ;

X1, Z1, FLAG, INC, COUNT : INTEGER ;

DELTAT, DELTAX, VEL, POS, ADD, HEIGHT : REAL ; ( DELTAT = time step,

DELTAX = mesh spacing )

TIME, X, Z : REAL ;

(

Initialization of arrays

)

PROCEDURE INIT(VAR MIX : MIX P;VAR VORT,SAI : NODE\_P;VAR U,W : VEL\_P;  
DELTAX : REAL);

VAR

I, J : INTEGER ;

Uo : REAL ; ( Uo = entrance horizontal velocity )

BEGIN

Uo := 10.00;

FOR J:=0 TO 20 DO

BEGIN

FOR I:=0 TO 60 DO

BEGIN

MIX^[I,J] := 0.0;

VORT^[I,J,1] := 0.0;

VORT^[I,J,2] := 0.0;

IF J#0 THEN

BEGIN

SAI^[I,J,1] := 0.0;

SAI^[I,J,2] := 0.0;

END;

END;

END;

FOR J:=1 TO 20 DO

BEGIN

SAI^[0,J,1] := SAI^[0,J-1,1]\*Uo;

SAI^[0,J,2] := SAI^[0,J,1];

FOR K:=1 TO 2 DO

BEGIN

FOR I:=1 TO 60 DO SAI^[0,J,K] := SAI^[0,J,1];

END;

END;

```

END;
FOR I:=0 TO 60 DO
BEGIN
  SAI^[I,20,1] := SAI^[0,20,1];
  SAI^[I,20,2] := SAI^[0,20,1];
END;
FOR I:=-2 TO 120 DO
BEGIN
  FOR J:=-2 TO 40 DO
  BEGIN
    U^[I,J] := Uo;
    W^[I,J] := 0.0;
  END;
END;
END;
(
  Display of Array Values
)
PROCEDURE DISPLAY ( M : NODE_P ; NEWN : INTEGER );
BEGIN
  FOR J:=20 DOWNT0 0 DO
  BEGIN
    GOTOXY (2,22-J);
    FOR I:=53 TO 60 DO WRITE ( W^[I,J,NEWN]:9:3 );
  END;
END;
(
  Storage of Array Values
)
PROCEDURE PMATRIX ( M : NODE_P ; NEWN : INTEGER );
VAR
  I, J, K : INTEGER ;
BEGIN
  FOR K:=0 TO 2 DO
  BEGIN
    J := 7 * K;
    FOR I:=0 TO 60 DO WRITELN ( OUT, W^[I,J,NEWN]:10:6, W^[I,J+1,NEWN]:10:6,
      W^[I,J+2,NEWN]:10:6, W^[I,J+3,NEWN]:10:6,
      W^[I,J+4,NEWN]:10:6, W^[I,J+5,NEWN]:10:6,
      W^[I,J+6,NEWN]:10:6 );
  END;
END;
(
  Storage of Array Values
)
PROCEDURE PMATRY2 ( M2 : VEL_P );
VAR
  I, J, K : INTEGER ;
BEGIN
  FOR K:=0 TO 2 DO
  BEGIN
    J := 7 * K;
    FOR I:=0 TO 60 DO WRITELN ( OUT, M2^[2+I,2+J]:10:6, M2^[2+I,2+J+2]:10:6,
      M2^[2+I,2+J+4]:10:6, M2^[2+I,2+J+6]:10:6,
      M2^[2+I,2+J+8]:10:6, M2^[2+I,2+J+10]:10:6,
      M2^[2+I,2+J+12]:10:6 );
  END;
END;
(
  Storage of Array Values
)
PROCEDURE PMATRY3 ( M3 : MIX_P );
VAR
  I, J, K : INTEGER ;

```

```

BEGIN
  FOR K:=0 TO 2 DO
    BEGIN
      J := 7 + K;
      FOR I:=0 TO 60 DO WRITELN ( OUT, M3^[I,J]:10:6, M3^[I,J+1]:10:6,
        M3^[I,J+2]:10:6, M3^[I,J+3]:10:6, M3^[I,J+4]:10:6,
        M3^[I,J+5]:10:6, M3^[I,J+6]:10:6 );
    END;
  END;
  (
    Storage of Particle Zone Outline
  )
  PROCEDURE PRZONE ( XPOS, ZPOS : PART_P );
  VAR
    J, K : INTEGER ;
    DX, DZ : REAL ;
  BEGIN
    WRITELN ( OUT, 'PR ZONE POSITIONS' );
    FOR K:=761 TO 800
      BEGIN
        DX := XPOS^K / 500.0 ;
        DZ := ZPOS^K / 500.0 ;
        WRITELN ( OUT, DX:10:4, DZ:10:4 );
      END;
    FOR J:=19 DOWNTO 2 DO
      BEGIN
        K := 40 * J;
        DX := XPOS^K / 500.0 ;
        DZ := ZPOS^K / 500.0 ;
        WRITELN ( OUT, DX:10:4, DZ:10:4 );
      END;
    FOR K:=40 DOWNTO 1 DO
      BEGIN
        DX := XPOS^K / 500.0 ;
        DZ := ZPOS^K / 500.0 ;
        WRITELN ( OUT, DX:10:4, DZ:10:4 );
      END;
    WRITELN ( OUT );
    FOR J:=2 TO 19 DO
      BEGIN
        K := ( 40 * J ) - 39 ;
        DX := XPOS^K / 500.0 ;
        DZ := ZPOS^K / 500.0 ;
        WRITELN ( OUT, DX:10:4, DZ:10:4 );
      END;
    END;
  (
    Graphical Display of Particle Zone
  )
  PROCEDURE VIEW(XPOS, ZPOS : PART_P; DELTAX : REAL; VAR XMEAN, ZMEAN : CENTROID;
    T : INTEGER );
  VAR
    K, IX, IZ : INTEGER ;
    MULT : REAL ;
  BEGIN
    HIRSCOLOR (3);
    DRAW (0,0,599,0,1);
    DRAW (0,199,599,199,1);
    DRAW (0,0,0,199,1);
    DRAW (599,199,599,0,1);
    MULT := 10.0 / DELTAX ;
    XMEAN(T) := 0.0 ;
    ZMEAN(T) := 0.0 ;
    FOR K:=1 TO 800 DO
      BEGIN
        IF XPOS^K ( 0.0 THEN XPOS^K := 0.0 ;
        IF XPOS^K ) 30000.0 THEN XPOS^K := 30000.0 ;

```

```

IF ZPOS^K ( 0.0 THEN ZPOS^K := 0.0 ;
XX := ROUND ( XPOS^K * MULT ) - 1 ;
ZZ := 199 - ROUND ( ZPOS^K * MULT ) ;
PLOT (XX,ZZ,1);
XMEAN(T) := XMEAN(T) + XPOS^K ;
ZMEAN(T) := ZMEAN(T) + ZPOS^K ;
END;
XMEAN(T) := XMEAN(T) / ( DELTAX * 800.0 ) ;
ZMEAN(T) := ZMEAN(T) / ( DELTAX * 800.0 ) ;
GOTOXY (63,23);
WRITE ( XMEAN(T):10:3 );
GOTOXY (63,24);
WRITE ( ZMEAN(T):10:3 );
END;
(
Subroutine for interpolation between node values
)
PROCEDURE INTERP_4 (VAR VAL_P, VAL_P1, VAL_P2, VAL_P3, VAL_P4, X, Z : REAL;
X1, Z1 : INTEGER );
VAR
CONSTA, VAL_PL, VAL_PR : REAL ;
BEGIN
CONSTA := Z - Z1 ;
VAL_PL := ( CONSTA * ( VAL_P2 - VAL_P1 ) ) + VAL_P1 ;
VAL_PR := ( CONSTA * ( VAL_P4 - VAL_P3 ) ) + VAL_P3 ;
VAL_P := ( ( X - X1 ) * ( VAL_PR - VAL_PL ) ) + VAL_PL ;
END;
(
Subroutine for calculation of new mixing ratios
)
PROCEDURE NEWMIX (VAR MIX : MIX_P; U, W : VEL_P; VAR XPOS, ZPOS : PART_P;
DELTAT, DELTAX, VEL : REAL );
VAR
I, J, K, X1, Z1, XX, ZZ, FLAG : INTEGER ;
X, Z, U_POINT, W_POINT, X_TRAVEL : REAL ;
Z_TRAVEL, ADD : REAL ;
BEGIN
FOR I:=0 TO 60 DO ( Paset matrix to 0 )
BEGIN
FOR J:=0 TO 20 DO MIX^I,J := 0.0;
END;
FOR K:=1 TO 800 DO
BEGIN
X := 2.0 * XPOS^K / DELTAX ;
Z := 2.0 * ZPOS^K / DELTAX ;
X1 := TRUNC ( X );
Z1 := TRUNC ( Z );
( Find velocity components at tracer locations )
INTERP_4 (U_POINT, U^X1,Z1, U^X1+1,Z1, U^X1+1,Z1+1, U^X1+1,Z1+1, X, Z, X1, Z1);
INTERP_4 (W_POINT, W^X1,Z1, W^X1,Z1+1, W^X1+1,Z1, W^X1+1,Z1+1, X, Z, X1, Z1);
( Determine distance of tracer travel during time step )
X_TRAVEL := U_POINT * DELTAT ;
Z_TRAVEL := ( W_POINT - VEL ) * DELTAT ;
( Calculate new tracer positions )
XPOS^K := XPOS^K + X_TRAVEL ;
ZPOS^K := ZPOS^K + Z_TRAVEL ;
( Tracers must be kept in boundary area )
IF XPOS^K ( 0.0 THEN XPOS^K := 0.0 ;
IF XPOS^K ( 30000.0 THEN XPOS^K := 30000.0 ;
IF ZPOS^K ( 0.0 THEN ZPOS^K := 0.0 ;
( Determination of new mixing ratios at each node )
X1 := ROUND ( ( XPOS^K ) / DELTAX ) ;
Z1 := ROUND ( ( ZPOS^K ) / DELTAX ) ;
FLAG := 0 ;
ADD := 0.0004 ;
IF FRAC ( XPOS^K / DELTAX ) = 0.5 THEN
BEGIN
ADD := ADD * 0.5 ;
FLAG := FLAG * 1 ;
END;
IF FRAC ( ZPOS^K / DELTAX ) = 0.5 THEN

```

```

BEGIN
  ADD := ADD + 0.5 ;
  FLAG := FLAG + 2 ;
END;
IF FLAG = 0 THEN MIX^CX1,Z11 := MIX^CX1,Z11 + ADD ;
IF FLAG = 1 THEN
BEGIN
  MIX^CX1,Z11 := MIX^CX1,Z11 + ADD ;
  MIX^CX1-1,Z11 := MIX^CX1-1,Z11 + ADD ;
END;
IF FLAG = 2 THEN
BEGIN
  MIX^CX1,Z11 := MIX^CX1,Z11 + ADD ;
  MIX^CX1,Z1-11 := MIX^CX1,Z1-11 + ADD ;
END;
IF FLAG = 3 THEN
BEGIN
  MIX^CX1,Z11 := MIX^CX1,Z11 + ADD ;
  MIX^CX1-1,Z11 := MIX^CX1-1,Z11 + ADD ;
  MIX^CX1,Z1-11 := MIX^CX1,Z1-11 + ADD ;
  MIX^CX1-1,Z1-11 := MIX^CX1-1,Z1-11 + ADD ;
END;
END;
END;
(
  Subroutine to calculate new vorticities for the mesh
)
PROCEDURE NEWVORT(MIX,VIS : MIX_P;VAR VORT : NODE_P;U,W : VEL_P;
  DELTAT,DELTA : REAL;NEWSM,OLD : INTEGER);
VAR
  I, J : INTEGER ;
  GRAVITY, SUM1, SUM2, SUM3, SUM4, DELTA : REAL ;
BEGIN
  GRAVITY := 0.00981 ;
  (
    Solution to vorticity transport equation
  )
  FOR J:=1 TO 19 DO
  BEGIN
    FOR I:=1 TO 59 DO
    BEGIN
      (
        Equation broken up to utilize co-processor
      )
      SUM1 := 0.5*GRAVITY*(MIX^CX1+1,J1-MIX^CX1-1,J1);
      SUM2 := 4.0*VORT^CX1,J,OLD ;
      SUM2 := VORT^CX1+1,J,OLD+VORT^CX1-1,J,OLD+VORT^CX1,J+1,OLD+
        VORT^CX1,J-1,OLD-SUM2;
      SUM2 := VIS^CX1,J1*SUM2/DELTA;
      SUM3 := 0.5*U^CX2+1,2*J*(VORT^CX1,J-1,OLD-VORT^CX1,J+1,OLD);
      SUM4 := 0.5*U^CX2+1,2*J*(VORT^CX1-1,J,OLD-VORT^CX1+1,J,OLD);
      SUM4 := SUM1+SUM2+SUM3+SUM4;
      DELTA := DELTAT+SUM4/DELTA;
      VORT^CX1,J,NEWSM := VORT^CX1,J,OLD+DELTA;
    END;
  END;
END;
(
  Subroutine to determine new stream function values using
  the SOR method with alternating sweep direction
)
PROCEDURE NEWSAI ( VAR SAI, VORT : NODE_P ; DELTA : REAL ; VAR NEWSM, NEWSB : INTEGER );
VAR
  I, J, COUNT, OLDB, FLAG : INTEGER ;
  DIF, SUM1, SUM2, DELTA, OMEGA : REAL ;
BEGIN
  OMEGA := 1.85 ; ( Optimized over relaxation factor )
  COUNT := 0 ;
  OLDB := 3 - NEWSB ;
  FLAG := 1 ;
  WHILE ( COUNT ( 400 ) AND ( FLAG ) 0 ) DO
  BEGIN
    DIF := 0.0 ;
    FLAG := 0 ;
    (
      Positive I-dir. sweep
    )
    IF NEWSB = 1 THEN

```

```

BEGIN
  FOR J:=1 TO 19 DO
    BEGIN
      SAI^(60,J,NEWB) := SAI^(59,J,OLDB);
      SAI^(0,J,NEWB) := SAI^(1,J,OLDB);
      FOR I:=1 TO 59 DO
        BEGIN
          SUM1 := VORT^(I,J,NEWB)+SOR(DELTA);
          SUM2 := 4.0*SAI^(I,J,OLDB);
          SUM2 := SAI^(I+1,J,OLDB)+SAI^(I,J+1,OLDB)+SAI^(I-1,J,NEWB)
                +SAI^(I,J-1,NEWB)-SUM1-SUM2;
          DELTA := OMEGA*SUM2/4.0;
          SAI^(I,J,NEWB) := SAI^(I,J,OLDB)+DELTA;
        END;
      END;
    END;
  ( Negative X-dir. sweep )
  ELSE
  BEGIN
    FOR J:=1 TO 19 DO
      BEGIN
        SAI^(60,J,NEWB) := SAI^(59,J,OLDB);
        SAI^(0,J,NEWB) := SAI^(1,J,OLDB);
        FOR I:=59 DOWNTO 1 DO
          BEGIN
            SUM1 := VORT^(I,J,NEWB)+SOR(DELTA);
            SUM2 := 4.0*SAI^(I,J,OLDB);
            SUM2 := SAI^(I+1,J,NEWB)+SAI^(I,J+1,OLDB)+SAI^(I-1,J,OLDB)
                  +SAI^(I,J-1,NEWB)-SUM1-SUM2;
            DELTA := OMEGA*SUM2/4.0;
            SAI^(I,J,NEWB) := SAI^(I,J,OLDB)+DELTA;
          END;
        END;
      END;
    ( Check for convergence )
    FOR J:=1 TO 19 DO
      BEGIN
        FOR I:=1 TO 59 DO
          BEGIN
            IF FLAG ( 1 ) THEN
              BEGIN
                DELTA := ABS(SAI^(I,J,NEWB)-SAI^(I,J,OLDB));
                IF DELTA > 0.01 THEN FLAG := 1;
              END;
            END;
          END;
        ( DISPLAY(SA:NEWB);
        NEWB := OLDB;
        OLDB := 3-OLDB;
        COUNT := COUNT+1;
        BOTOXY (24,24);
        WRITELN('SOR Method took ',COUNT:3,' iterations');
        END;
      END;
    ( Subroutine for calculation of X-dir. velocity field
    )
    PROCEDURE NEW_U(SAI ; NODE_P;VAR U ; VEL_P;NEWB ; INTEGER;DELTA ; REAL);
    VAR
      I, J ; INTEGER ;
    BEGIN
      FOR J:=0 TO 19 DO
        BEGIN
          FOR I:=1 TO 59 DO U^(2+I,2+J+1) := SAI^(I,J+1,NEWB)-SAI^(I,J,NEWB);
        END;
        FOR J:=1 TO 19 DO U^(120,2+J) := U^(19,2+J);
        FOR I:=1 TO 59 DO
          BEGIN
            U^(2+I,40) := U^(2+I,39);
            FOR J:=1 TO 19 DO U^(2+I,2+J) := (U^(2+I,2+J+1)-U^(2+I,2+J-1))/2.0
                  +U^(2+I,2+J-1);
          END;
        FOR J:=1 TO 19 DO U^(-2,2+J) := 0.0-U^(2,2+J);

```

```

FOR J:=0 TO 40 DO
  BEGIN
    FOR I:=0 TO 59 DO U^(2*I+1,J) := (U^(2*I+2,J)-U^(2*I,J))/2.0+U^(2*I,J);
  END;
END;
(
  Subroutine for calculation of Z-dir. velocity field
)
PROCEDURE NEW_W(SAI : NODE_P;VAR W : VEL_P;NEWB : INTEGER;DELTA : REAL);
VAR
  I, J : INTEGER ;
BEGIN
  FOR I:=0 TO 59 DO
    BEGIN
      FOR J:=1 TO 19 DO W^(2*I+1,2*J) := SAI^(I,J,NEWB)-SAI^(I+1,J,NEWB);
    END;
    FOR J:=1 TO 19 DO
      BEGIN
        W^(0,2*J) := W^(1,2*J);
        W^(120,2*J) := W^(119,2*J);
        FOR I:=1 TO 59 DO W^(2*I,2*J) := (W^(2*I+1,2*J)-W^(2*I-1,2*J))/2.0
          +W^(2*I-1,2*J);
        W^(-2,2*J) := W^(2,2*J);
      END;
    FOR I:=0 TO 120 DO
      BEGIN
        FOR J:=0 TO 19 DO W^(I,2*J+1) := (W^(I,2*J+2)-W^(I,2*J))/2.0+W^(I,2*J);
      END;
    END;
  (
    Calculation of vorticity at slip wall
  )
  PROCEDURE VORTBC (VAR VORT : NODE_P;NEWM : INTEGER);
  VAR
    I : INTEGER ;
  BEGIN
    FOR I:=1 TO 59 DO VORT^(I,0,NEWM) := VORT^(I,1,NEWM);
  END;
  PROCEDURE SIGNAL ;
  BEGIN
    SOUND (440);
    DELAY (500);
    NOSOUND ;
    DELAY (50);
    SOUND (500);
    DELAY (500);
    NOSOUND ;
    DELAY (50);
    SOUND (320);
    DELAY (500);
    NOSOUND ;
  END;
  BEGIN
    NEW (MIX);
    NEW (VIS);
    NEW (VORT);
    NEW (SAI);
    NEW (U);
    NEW (W);
    NEW (XPOS);
    NEW (ZPOS);
    (
      Initialization of viscosity field
    )
    FOR I:=0 TO 60 DO
      BEGIN
        FOR J:=0 TO 20 DO VIS^(I,J) := 1000.0 ;
      END;
    END;
    (
      Setting of parameters
    )
    VEL := 6.1 ;
    DELTAT := 25.0 ;
    DELTAX := 500.0 ;
    OLD := 2 ;
    NEWM := 1 ;
  END;

```

```

NEWB := 3 ;
INC := 1 ;
COUNT := 1 ;
INIT ( MIX, VORT, SAI, U, W, DELTAX ) ;
( Creation of zone tracer particles )
FOR J:=0 TO 19 DO
BEGIN
FOR I:=1 TO 40 DO
BEGIN
POS := ( I * 100.0 ) + 9950.0 ;
K := ( 40 * J ) + I ;
XPOS*(K) := POS ;
END;
END;
FOR I:=0 TO 39 DO
BEGIN
FOR J:=1 TO 20 DO
BEGIN
POS := ( J * 100.0 ) + 6950.0 ;
K := ( 40 * ( J - 1 ) ) + I + 1 ;
ZPOS*(K) := POS ;
END;
END;
( Calculation of initial mixing ratios )
FOR K:=1 TO 800 DO
BEGIN
X := XPOS*(K) / DELTAX ;
Z := ZPOS*(K) / DELTAX ;
X1 := TRUNC (X);
Z1 := TRUNC (Z);
FLAG := 0 ;
ADD := 0.0004 ;
IF FRAC (X) = 0.5 THEN
BEGIN
ADD := ADD * 0.5 ;
FLAG := FLAG + 1 ;
END;
IF FRAC (Z) = 0.5 THEN
BEGIN
ADD := ADD * 0.5 ;
FLAG := FLAG + 2 ;
END;
IF FLAG = 0 THEN MIX*(X1,Z1) := MIX*(X1,Z1) + ADD ;
IF FLAG = 1 THEN
BEGIN
MIX*(X1,Z1) := MIX*(X1,Z1) + ADD ;
MIX*(X1-1,Z1) := MIX*(X1-1,Z1) + ADD ;
END;
IF FLAG = 2 THEN
BEGIN
MIX*(X1,Z1) := MIX*(X1,Z1) + ADD ;
MIX*(X1,Z1-1) := MIX*(X1,Z1-1) + ADD ;
END;
IF FLAG = 3 THEN
BEGIN
MIX*(X1,Z1) := MIX*(X1,Z1) + ADD ;
MIX*(X1-1,Z1) := MIX*(X1-1,Z1) + ADD ;
MIX*(X1,Z1-1) := MIX*(X1,Z1-1) + ADD ;
MIX*(X1-1,Z1-1) := MIX*(X1-1,Z1-1) + ADD ;
END;
END;
VIEW ( XPOS, ZPOS, DELTAX, XMEAN, ZMEAN, 0 ) ;
( Stepping loop through time )
FOR K:=1 TO 36 DO
BEGIN
TIME := DELTAT * K ;
OLD := 3 - OLD ;
NEWB := 3 - NEWB ;
NEWMIX = MIX, U, W, XPOS, ZPOS, DELTAT, DELTAX, VEL ;
VIEW ( XPOS, ZPOS, DELTAX, XMEAN, ZMEAN, K ) ;
GOTOX (76,1) ;

```

```

GOTOXY (76,1);
WRITE ( TIME:4:1 );
NEWVORT ( MIX, VIS, VORT, U, W, DELTAT, DELTAX, NEWW, OLD );
VORTBC ( VORT, NEWW );
NEWSAI ( SAI, VORT, DELTAX, NEWW, NEWB );
NEW U ( SAI, U, NEWB, DELTAX );
NEW W ( SAI, W, NEWB, DELTAX );
( Storing of output )
IF INC = 12 THEN
BEGIN
IF COUNT = 1 THEN ASSIGN ( OUT, '300.100' );
IF COUNT = 2 THEN ASSIGN ( OUT, '600.100' );
IF COUNT = 3 THEN ASSIGN ( OUT, '900.100' );
REWRITE ( OUT );
WRITE ( OUT, ' Matrix Elements at ', TIME:5:1, ' Seconds' );
WRITE ( OUT, ' ');
WRITE ( OUT, ' MIXING RATIOS' );
PRMATRIX ( MIX );
WRITE ( OUT, ' VORTICITIES' );
PRMATRIX ( VORT, NEWW );
WRITE ( OUT, ' STREAM FUNCTIONS' );
PRMATRIX ( SAI, NEWB );
WRITE ( OUT, ' X-DIRECTION VELOCITIES' );
PRMATRIX ( U );
WRITE ( OUT, ' Z-DIRECTION VELOCITIES' );
PRMATRIX ( W );
PRZONE ( XPOS, ZPOS );
INC := 0 ;
COUNT := COUNT + 1 ;
CLOSE ( OUT );
END ;
INC := INC + 1 ;
END ;
ASSIGN ( OUT, 'CENTER.100' );
REWRITE ( OUT );
WRITE ( OUT, ' ZONE CENTROID ( X,Z )' );
FOR I:=0 TO 40 DO WRITE ( OUT, 'XMEANCI:10:2, ' ', ZMEANCI:10:2 );
CLOSE ( OUT );
SIGNL ;
CLOSE ( OUT );
GOTOXY (78,24);
END.

```